Influence of Stator Gap on Electromagnetic Performance of 6-Slot/2-Pole Modular High Speed Permanent Magnet Motor With Toroidal Windings

F. XU[1], Z. Q. ZHU [1], (Fellow, IEEE), T. R. HE[1], Y. WANG [1], H. BIN[2], D. WU[2], (Member, IEEE), L. M. GONG[2], (Senior Member, IEEE), AND J. T. CHEN[2], (Senior Member, IEEE)

[1]Department of Electronic and Electrical Engineering, The University of Sheffield, Sheffield S1 3JD, U.K.
[2]Motors and Drives Center, Midea Group Corporate Research Center, Shanghai 201203, China

Corresponding author: Z. Q. Zhu (z.q.zhu@sheffield.ac.uk)

ABSTRACT The 6-slot/2-pole (6s/2p) permanent magnet motors with a diametrically magnetized PM rotor are popular for high speed application. Meanwhile, toroidal winding can not only reduce end-winding length but also eliminate unbalanced magnetic force for short axial length motors. Therefore, the electromagnetic performance of a 6s/2p high speed PM (HSPM) motor with toroidal windings is firstly analyzed, including air-gap flux density, flux linkage, back-EMF, cogging torque and electromagnetic torque. Then, considering modular design for auto-manufacturing, the influence of stator gap and misalignment on the electromagnetic performance is investigated. It shows that the stator gap results in unbalanced three phase back-EMFs, not only amplitudes, but also phase angles. The stator gap increases the equivalent air-gap length and PM flux leakage, which leads to lower air-gap flux density, back-EMF, and average torque. Moreover, the stator gap results in asymmetric air-gap length, which results in large cogging torque. Further, it shows that the misalignment of two stator parts mainly affects the uneven equivalent air-gap length and symmetry of winding configuration, which leads to unbalanced three phase back-EMFs, especially phase angles, and self- and mutual-inductances, as well as rotor PM loss. Experimental results of a prototype motor with/without stator gap and/or misalignment are given to validate the finite element predicted analyses.

INDEX TERMS High speed, permanent magnet machine, toroidal winding.

I. INTRODUCTION

High speed permanent magnet (PM) motors have been widely used for various applications and become more and more popular in recent years. Extensive researches have been carried out on high speed motors in terms of new motor topologies, design methodologies, modelling and analysis techniques of losses, thermal, and rotor stress, as well as application of new materials and development of new control strategies. For small size, high speed application, 6-slot/2-pole (6s/2p) high speed permanent magnet (HSPM) motors with concentrated tooth coil windings are employed widely due to short end-winding length and no unbalanced magnetic force [1]. In high speed operation, high aspect ratio due to long motor

The associate editor coordinating the review of this manuscript and approving it for publication was R. K. Saket .

axial length normally leads to a rotor dynamic issue and may cause the damage of the rotor [2]. Hence, besides the tooth coil with short end-winding length, the toroidal winding also becomes a popular design alternative for high speed application which demands a short motor axial length [1], [3]–[5]. They are widely adopted in low-power application whilst the operating speed normally exceeds 100krpm. In [3], a 100W, 500 krpm PM slotless machine with toroidal winding for gas turbines was designed and tested. The slotless toroidal winding is adopted to eliminate the rotor eddy-current loss due to no slotting effect. Such combination of slotless stator and toroidal winding can also be found in [4]. In [4], the 6s/2p HSPM motor with slotted tooth-coil winding and the 6s/2p HSPM slotless motor with toroidal winding were compared. It shows that slotless motor with toroidal winding has the highest efficiency and torque density when operating

at 150 000 rpm. In addition, this paper shows that the slotted motor has higher thermal capability and larger heat transfer coefficient. A 160 000 rpm millimeter-scale slotless bearing-less motor is presented in [5] to overcome the limitation of conventional ball bearings for high speed spindles applications.

Besides, compared with conventional distributed windings, toroidal windings are widely adopted to shorten end-winding and motor total axial length for high-power high-speed application [6]–[9]. Another merit of such toroidal windings is higher thermal dissipation capability due to the presence of extra air-duct.

On the other hand, the modular design is widely employed for manufacture automation. For tooth-coil windings, there are several modular designs have been researched. The influence on electromagnetic performance of modular stator has been investigated in [10], [11] such as stator tooth segments and back-iron segments. Different segmented stator core and manufacturing methods of motors with concentrated windings have been investigated in [12]. [13]–[16] have proposed a modular flux concentrating machine with segmented stator and rotor. In [11], the modularity techniques in PM machines with tooth-coil winding were comprehensively reviewed. In [17]–[19], the influence of modularity on the machine performance has been investigated and analyzed. Although several modularity techniques can be employed in toroidally-wound motors, the influence of modular design on the performance of motors with toroidal windings has never been investigated in literature and will be analyzed in this paper.

In this paper, the motor topology, winding factor and end-winding model of the 6s/2p HSPM motor with toroidal windings are illustrated in section II. In section III, the electromagnetic performances of the motor without stator gap are analyzed, including air-gap flux density, flux linkage, back-EMF, cogging torque and electromagnetic torque. Section IV investigates the influence of the stator gap on the performance of the 6s/2p HSPM toroidally-wound motor. Sections V and VI further investigate the influence of misalignment, as well as mixed stator gap and misalignment. Section VIII illustrates the potential influence of tooth tip. Section VIII provides extensive experimental results for a prototype motor with/without stator gap and/or misalignment to validate the finite element predicted results. Finally, the conclusion is given in section IX.

II. TOPOLOGIES OF HSPM MOTOR WITH TOROIDAL WINDINGS

The cross-sections of 6s/2p HSPM toroidally-wound motors without and with stator gap are presented in Fig.1. The stator gap is located between the windings of phase A and phase C, which divides stator into two halves which can ease the automated winding. To simplify the production, this 6-slot motor with straight teeth has no tooth tip, whose influence will also be investigated later in this paper. It is assumed that the sum of split teeth width in Fig.1 (b) is the same as that of one un-split tooth. The 2-pole rotor consists of two parts including
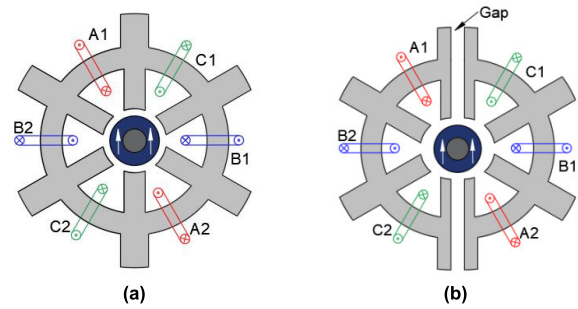

FIGURE 1. 6s/2p HSPM toroidal motors without and with stator gap. (a) Without gap. (b) With gap.

N45SH parallel magnetized magnet ring (or cylinder) and SUS430 magnetic shaft. The main parameters of 6s/2p HSPM motors without stator gap are given in Table 1.

TABLE 1. Main parameters of 6/2 HSPM motors without stator gap.

Rated current density (A/mm^2)	10	Air-gap length (mm)	1.55
Rated speed (krpm)	180	Rotor outer radius (mm)	5.25
Stator outer radius (mm)	27	Magnet thickness (mm)	2.75
Stator active length (mm)	8.6	Remanence (T)	1.3
Stator inner radius (mm)	6.8	Magnetization	Parallel
Stator yoke height (mm)	4.6	Number of turns per phase	32

A. WINDING FACTOR

For the toroidal winding, the calculation of winding factor is different from the conventional formulae for tooth wound winding. The winding factor of a 6s/2p PM motor with toroidal windings is only 0.5, which results from the product of pitch factor (=0.5) and distribution factor (=1) [20]. Both 6s/2p PM motors with tooth-wound and toroidal windings have no unbalanced magnetic force and the same winding factor (0.5), which is lower than that of 3-slot/2-pole tooth-wound windings (0.866) which has significant unbalanced magnetic force.

B. END-WINDING

The end-winding of the toroidally-wound motor is special. The outside conductors form the current loop, and can be treated as a part of end-winding length. In addition, the end-winding length also includes the axial part links the outside and inside conductors. In this paper, a semi-circular end-winding model is employed, Fig. 2. The total end-winding length (l_e) of one coil can be calculated as (1) [21].

$$l_e = 2\left[\frac{\pi}{2}\left(\frac{h_{out} + h_{in}}{2} + h_y\right)\right] + l_a \quad (1)$$

where h_{out} and h_{in} mean the outer and inner tooth heights, respectively. h_y is the yoke height. l_a is the stator active length.
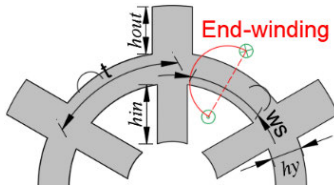
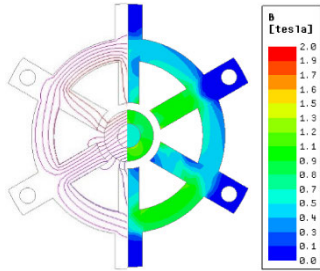**FIGURE 2. End-winding model.**

FIGURE 3. Flux distribution and equal potential of the 6s/2p HSPM toroidal motor without stator gap.
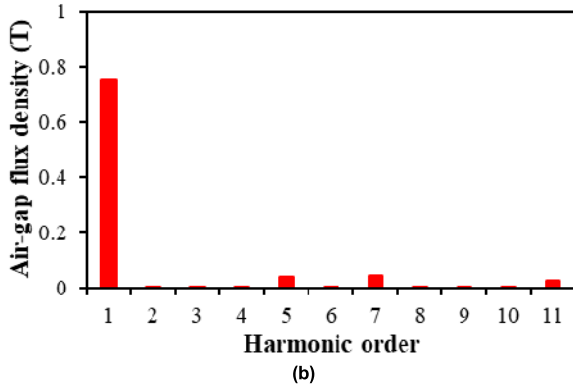

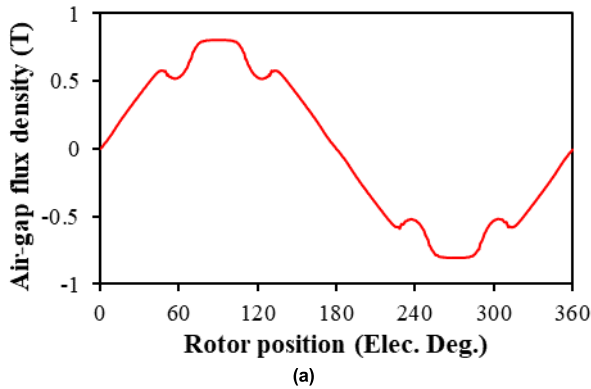**FIGURE 4. Open-circuit air-gap flux density of the motor without stator gap. (a) Waveform. (b) Harmonics.**
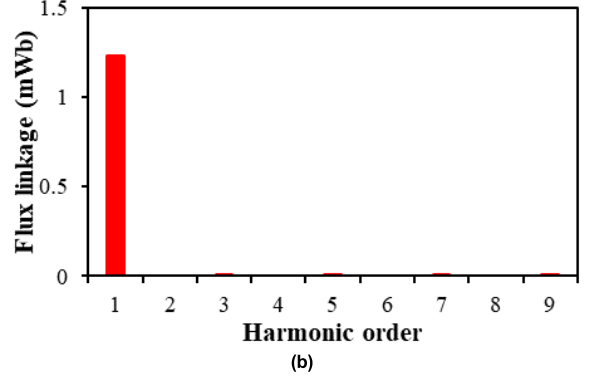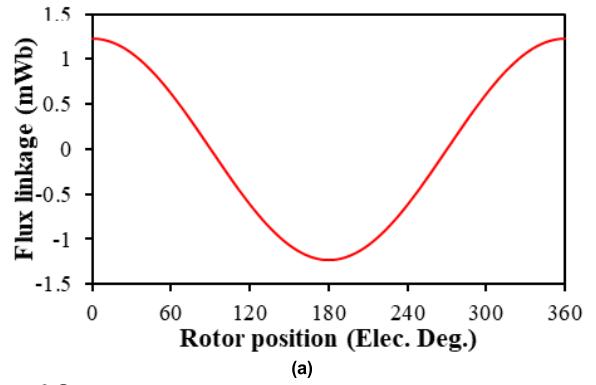

FIGURE 5. Flux linkage of phase A of the motor without stator gap. (a) Waveform. (b) Harmonics.
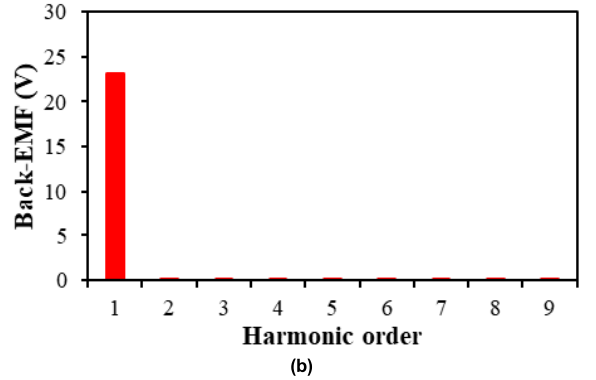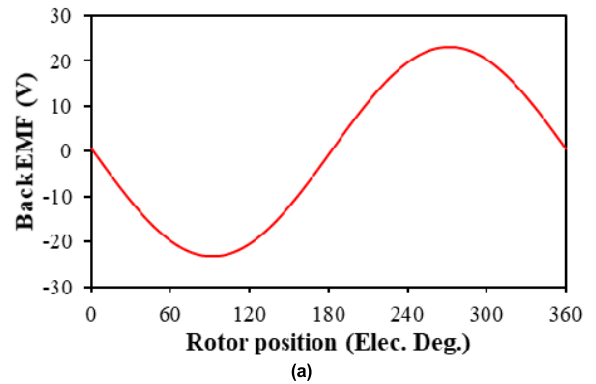
FIGURE 6. Back-EMF of phase A of the motor without stator gap. (a) Waveform. (b) Harmonics.

III. ELECTROMAGNETIC PERFORMANCE WITHOUT STATOR GAP

In this section, the electromagnetic performances of the 6s/2p motor without stator gap are analyzed, including air-gap flux density, flux linkage, back-EMF, cogging torque and electromagnetic torque. Fig. 3 shows the equal potential and flux density distributions of the motor without stator gap by the finite element analysis (FEA). It can be seen that there is almost no flux linking with the outside conductors (and this is why this part of conductors can be treated as a part of the end windings). Fig. 4 shows the air-gap flux

density waveform and spectrum. The air-gap flux density of the motor without stator gap is essentially sinusoidal due to diametrically magnetized PM. Meanwhile, the air-gap flux
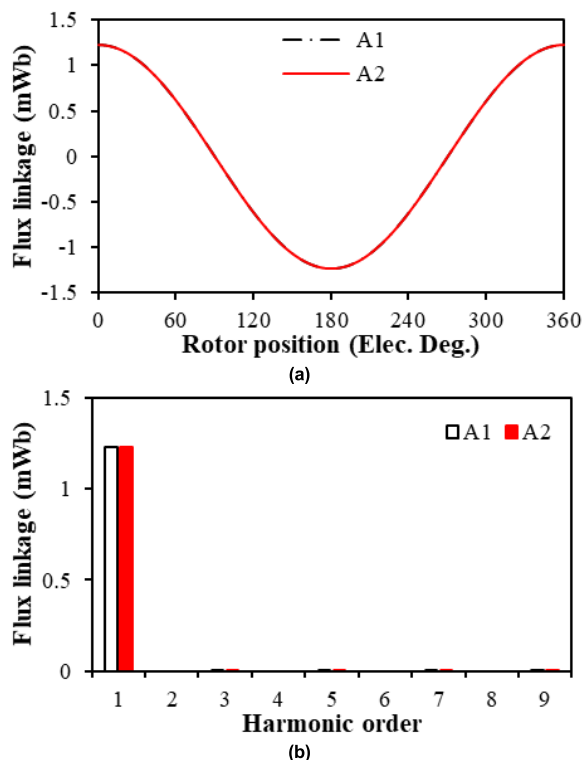
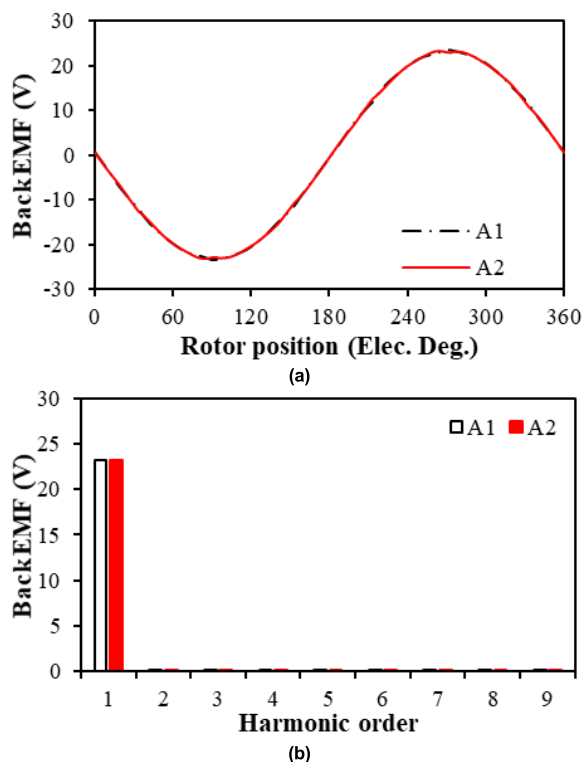**FIGURE 7.** Flux linkages of coil A1 and coil A2 of the motor without stator gap. (a) Waveforms. (b) Harmonics.

FIGURE 8. Back-EMFs of coil A1 and coil A2 of the motor without stator gap. (a) Waveforms. (b) Harmonics.

density also exists the 5th, 7th, 11th, 13th,... order harmonics due to slotting effect. The flux linkage and back-EMF of the motor without stator gap are shown in Fig. 5 and Fig. 6. The
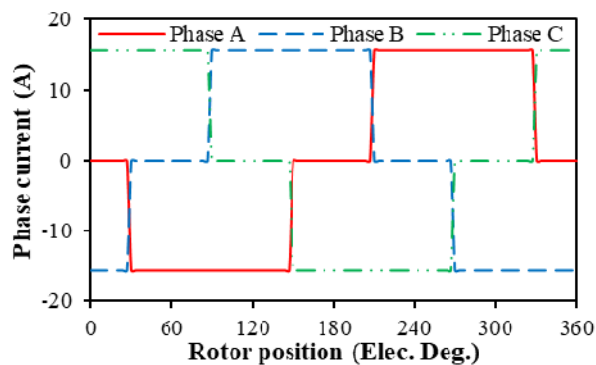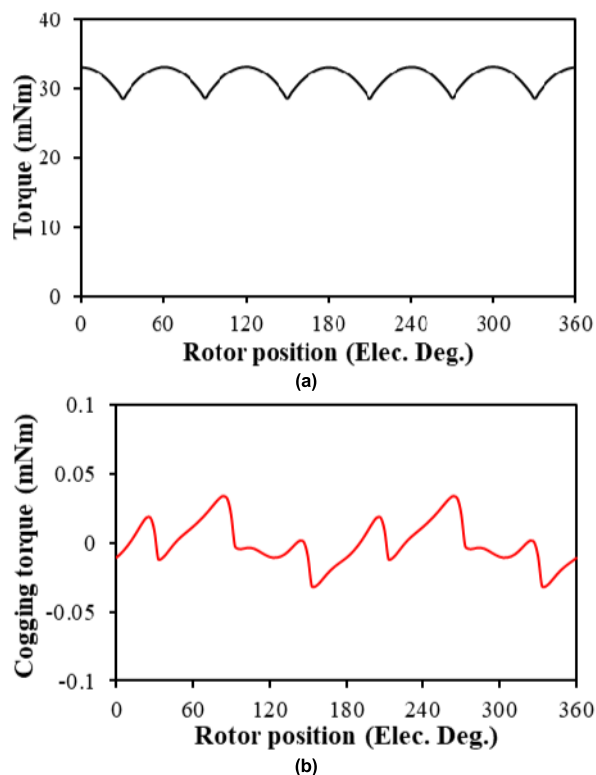

FIGURE 9. Ideal square phase current waveforms.

FIGURE 10. Torque of the motor without stator gap. (a) Electromagnetic torque. (b) Cogging torque.

waveforms are all sinusoidal and have negligible harmonics. Due to opposite connection polarities of the inside parts of coil A1 and coil A2, the harmonics are almost eliminated.

Under brushless direct current (BLDC) operation which is common for high speed operation, the ideal square BLDC current waveforms with the rated current density of 10A/mm^2 are illustrated in Fig. 9. Meanwhile, the electromagnetic torque and cogging torque waveforms are presented in Fig. 10. The results show that the motor without stator gap has almost no cogging torque, but has relatively large torque ripple, which results from the product of square BLDC currents and almost sinusoidal back-EMF waveforms.
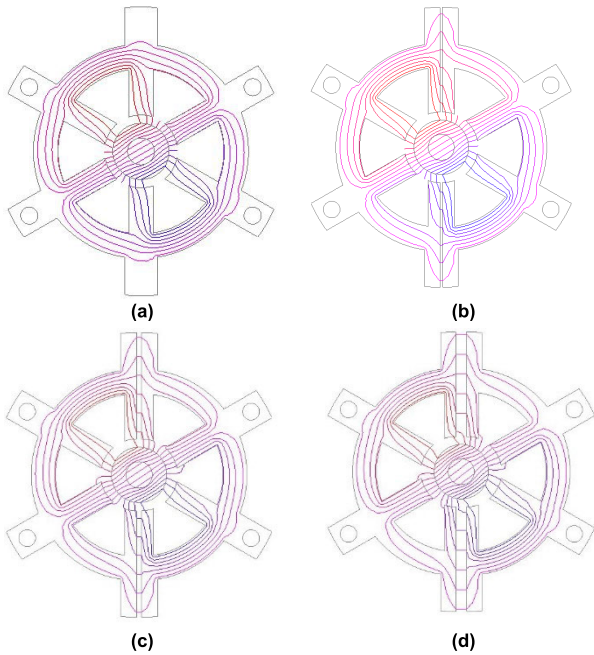
FIGURE 11. Equal potential distributions of 6s/2p HSPM toroidal wound motors with different stator gap. (a) 0mm. (b) 0.5mm. (c) 1mm. (d) 3mm.

IV. ELECTROMAGNETIC PERFORMANCE WITH STATOR GAP

To realize the modularity for automated winding, the stator is split into two parts. However, the modular design inevitably introduces the gaps in the stator, in Fig. 1(b). Generally, the presence of air-gap in the stator teeth increases the equivalent air-gap length of the motor thus making an impact on the electromagnetic performance. On the other hand, the actual slot number changes from six to eight due to the presence of two extra air gaps. The stator can be treated as a virtually whole stator with eight slot with uneven teeth and slot openings. Correspondingly, the stator slotting effect on the electromagnetic performance such as EMF and cogging torque may be significantly changed. Therefore, the influence of the stator gap on the electromagnetic performances will be comprehensively investigated in this section.

A. AIR-GAP FLUX DENSITY

The gap between split stators not only enlarges the equivalent air-gap but also results in uniform air-gap distribution of motor. Fig. 11 shows the open-circuit equal potential distributions of the motors with different stator gaps, i.e. 0, 1, 2, and 3 mm, although the stator gap is a bit exaggerated in order to reveal and appreciate its influence. Fig. 12 shows that the fundamental amplitude of air-gap flux density decreases with the increase of stator gap. This results from the increased average stator reluctance with the enlarged stator gaps. Meanwhile, amplitudes of the 5th, 7th, 11th, 13th order harmonics due to slotting effect decrease with the stator gap, as shown in Fig.12. The stator gap changes the slot number from 6 to 8, which means the field harmonics of the order (m $p\pm8$) occur, e.g., the 3rd, 9th, etc., as shown in Fig. 12(b).
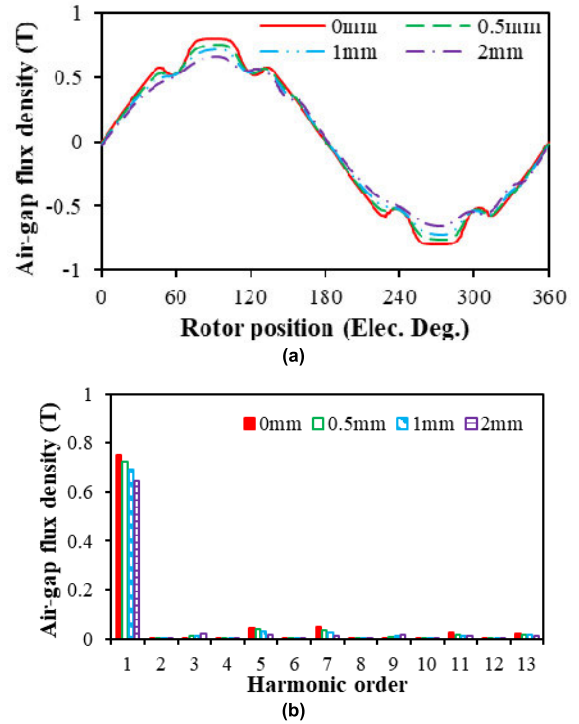

FIGURE 12. Air-gap flux density distributions of the motor with different stator gaps on circular path away from rotor by 0.775 mm. (a) Waveforms. (b) Harmonics.
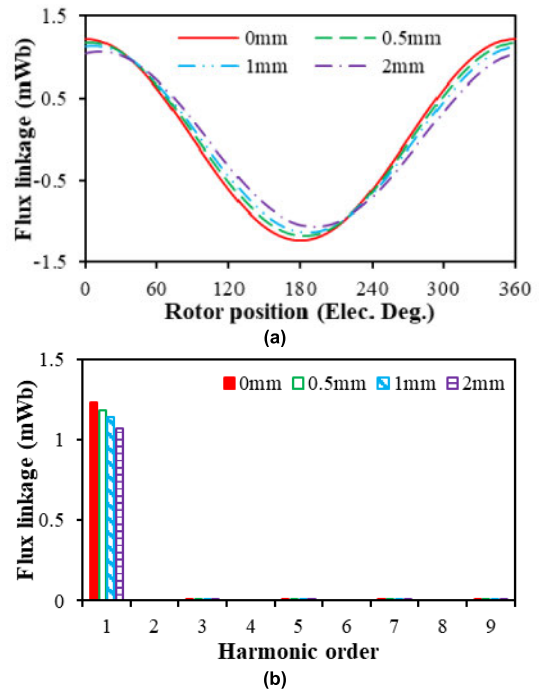

FIGURE 13. Flux linkage of phase A with different stator gaps. (a) Waveforms. (b) Harmonics.

B. FLUX LINKAGE

As mentioned in section A, the stator gap increases the leakage flux due to the increase of equivalent air-gap
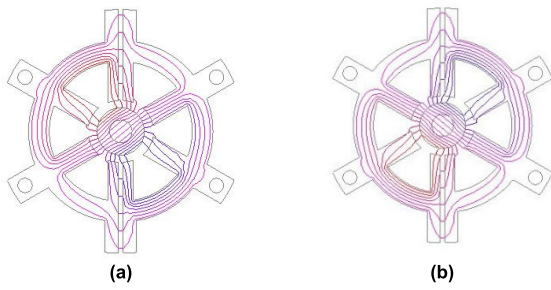
FIGURE 14. Equal flux potential distributions with the specific rotor positions for maximum flux linkage. (a) Phase A. (b) Phase C. Stator gap = 1mm.

FIGURE 15. Influence of stator gap on phase angle of flux linkage. (a) Phase angle. (b) Offset phase angle.
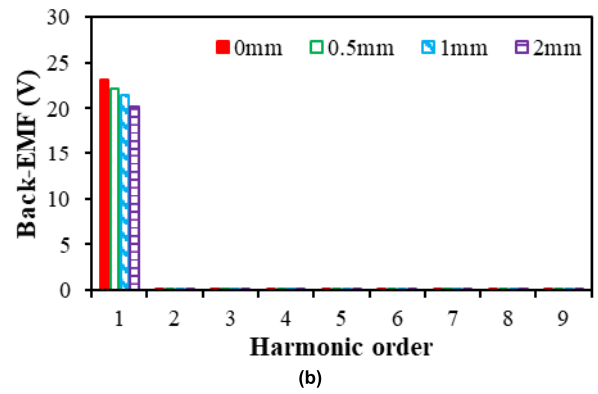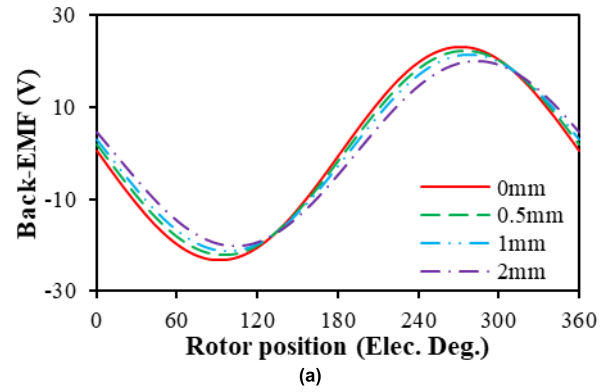

FIGURE 16. Back-EMFs of phase A with different stator gaps. (a) Waveforms. (b) Harmonics.

symmetrical. The variations of phase angles for phase A and phase C are opposite.

C. BACK-EMF

The back-EMF exhibits a similar trend with the flux linkage. As shown in Fig. 16, the stator gap decreases the amplitude of fundamental back-EMF, but does not introduce extra harmonic contents. More importantly, the stator gap affects the phase angle of three phase back-EMFs, which leads to the unbalanced three phase back-EMFs. In Fig. 17, when the stator gap is 3 mm, the phase angles of three phase back-EMFs do not differ by 120 electrical degrees. Compared with the motor without stator gap, phase A and phase C of the motor with stator gap have the lead and retard angles, but phase B keeps the same phase angle due to the stator gap location between phase A and phase C. Fig. 17 shows the influence of stator gap on the phase lead and retard angles. As mentioned before, the variation trends of back EMFs of phase A and phase C are opposite but the offset value remains the same.

D. COGGING TORQUE

Cogging torque is generated from the interaction between stator slots and rotor PM poles. Generally, the 6s/2p PM motor with parallel magnetized rotor should have negligible cogging torque. Significant cogging torque is produced due to the presence of stator gap. Fig. 18 and Fig. 19 show that
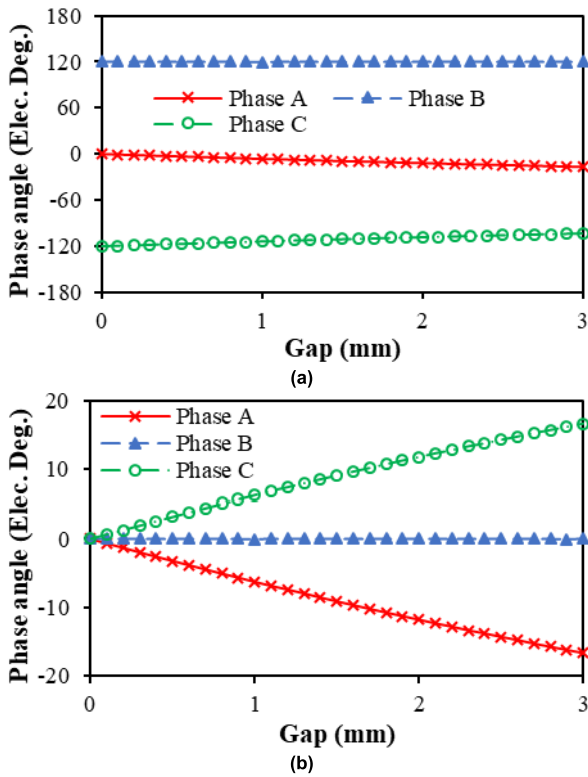
length. Therefore, the fundamental amplitude of flux linkage decreases with the increase length of stator gap. The introduction of stator gaps introduces almost no extra harmonics in the flux linkage, although the rotor positions where the amplitudes of flux linkage reach maximum and minimum are significantly altered, Fig. 13. Fig. 14 indicates equal potential distribution of the motor with 1mm stator gap at the specific rotor position when the flux linkage of phase A or phase C reaches the maximum. Phase angle of phase A is retarded and that for phase C is leaded. Fig. 15 illustrates the variation of phase angle of flux linkage with the increase of stator gap. The phase angle of phase B remains the same when the stator gap increases. The reason is that the stator gap is located between phase A and phase C, and both coils of phase B are
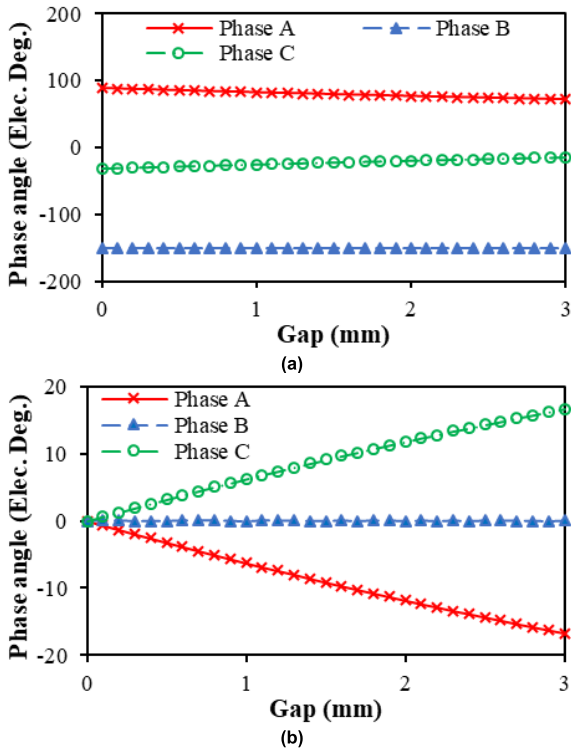
FIGURE 17. Influence of stator gap on phase angle of back EMF. (a) Phase angle. (b) Offset phase angle.
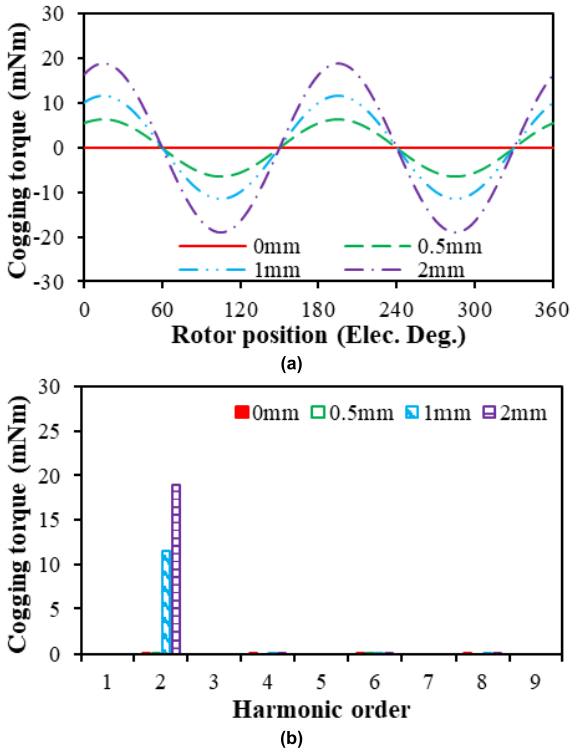

FIGURE 18. Cogging torque of the motor with different stator gaps. (a) Waveforms. (b) Harmonics.

the peak cogging torque rises with the increase of stator gap before reaching the maximum value and then drops afterwards. The maximum peak cogging torque can be achieved when the stator gap is 4.8 mm.
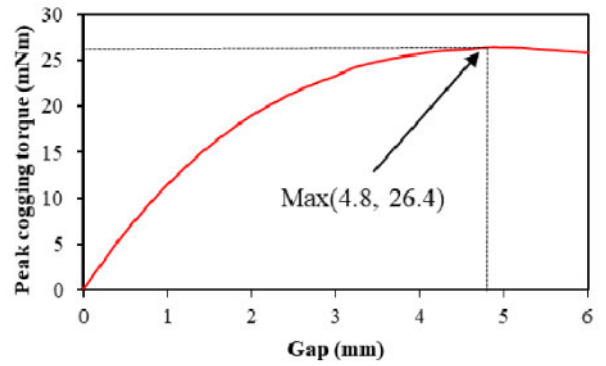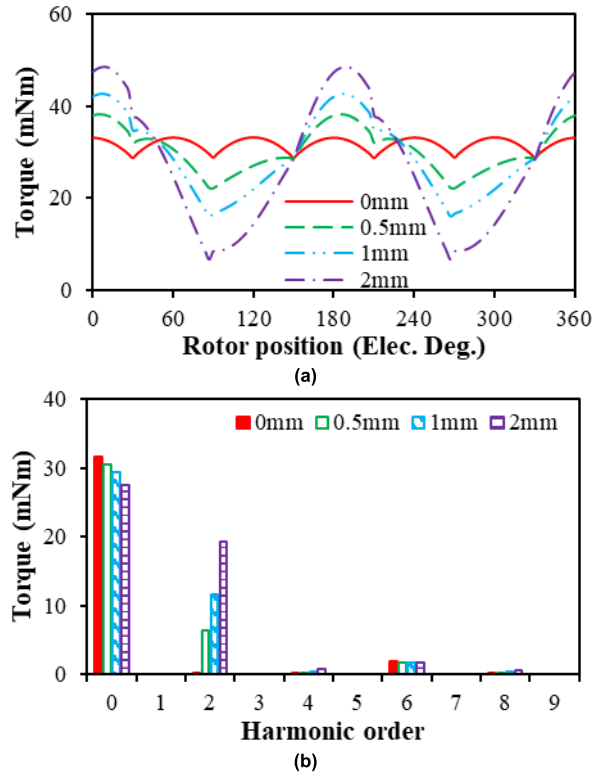

FIGURE 19. Influence of the stator gap on the peak cogging torque.

FIGURE 20. Torque of the motor with different stator gaps ($J = 10A/mm^2$). (a) Waveforms. (b) Harmonics.

E. ON-LOAD TORQUE

The influence of different stator gaps on the on-load torque of the motor with rated current density (10A/mm²), Fig. 20. It can be seen that the torque ripples increase significantly with the increase of the stator gap due to the increase of cogging torque. When the stator gap is larger than 3 mm, the on-load torque has negative values at several rotor positions, as shown in Figs. 20 and 21. Fig. 21 shows that when the stator gap is 3mm, the cogging torques are negative at several rotor positions, and the amplitudes of the negative cogging torque are larger than the electromagnetic torque at the same rotor position, which results in negative on-load torque. It is assumed that the influence of on-load condition on cogging
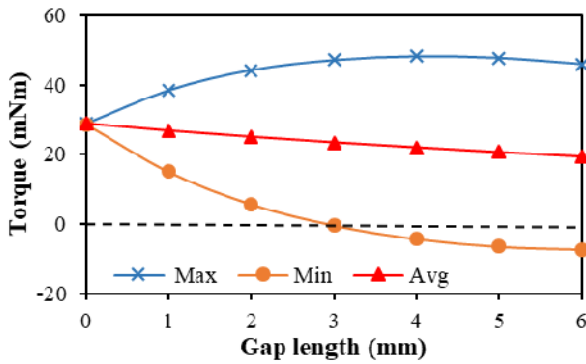
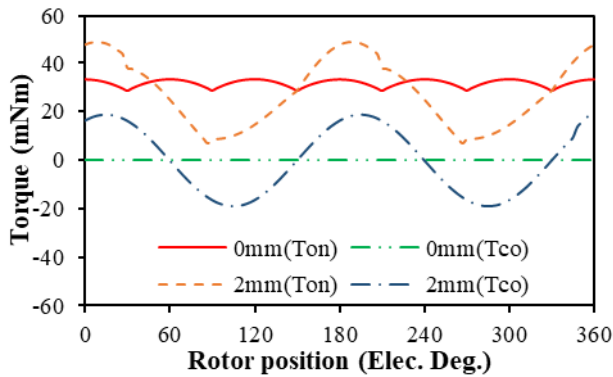**FIGURE 21.** Influence of stator gap on average torque.

FIGURE 22. Relationship between cogging torque and on-load torque of the motor with 2mm stator gap.

FIGURE 23. Inductances of the motor with different stator gaps. (a) Self-inductance. (b) Mutual-inductance.
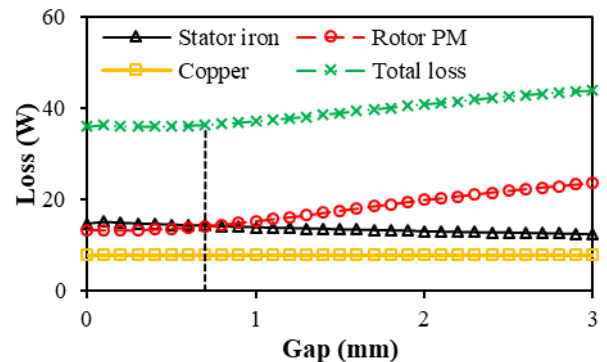
FIGURE 24. Loss of the motor with different stator gaps ($J = 10A/mm^2$, 180krpm).

torque is neglected. In addition, the stator gap affects not only the harmonic amplitudes, but also the harmonic contents, especially the 2nd harmonic which due to cogging torque, as shown in Fig. 20(b).

F. INDUCTANCE

High speed motors normally have small winding inductances. Even though there is a slight change of inductance due to the stator gap, the influence could be significant. The inductance is calculated by FEA, when only one phase excited ($I_a = 1A$, $I_b = 0A$, $I_c = 0A$). Since the stator gap is located between phase A and phase C, the self-inductance of phase B remains the same with the stator gap, but the self-inductances of phase A and phase C decrease, as shown in Fig. 23. The mutual-inductances between phase B, phase A and C decrease when the stator gap increases. However, the mutual-inductances of phase A to phase C increases.

G. LOSSES

Stator iron loss will be affected due to non-uniformed air-gap because of the gap between the stator. In this paper, the current density is fixed and the ac effect on the copper loss is neglected. In high speed motor, due to the poor thermal dissipation capability, the rotor temperature rise caused by the rotor eddy current loss should be considered. High rotor
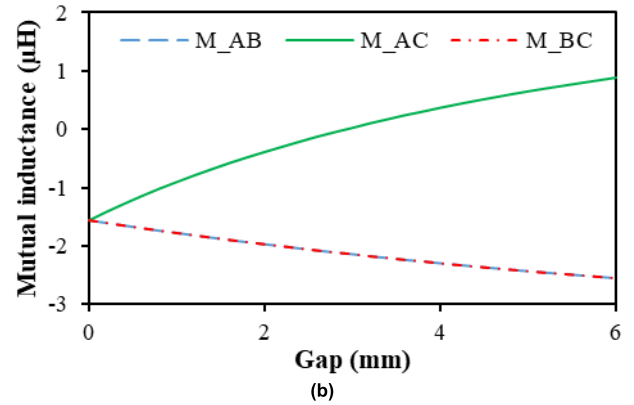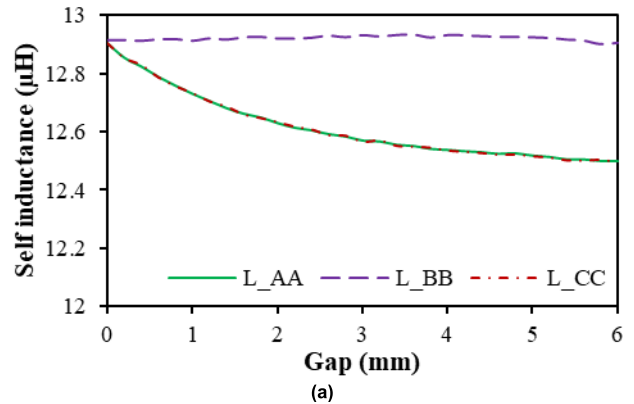
temperature may result in irreversible demagnetization and damage the rotor bearing system. With the increase of stator gap, dc copper loss keeps the same, the stator iron loss increases and the rotor PM loss decreases, Fig. 24. It can conclude that the stator gap below 1mm has almost no effect on the losses.

1) STATOR IRON LOSS

Generally, the iron loss can be calculated using the Bertotti model [22], [23]:

$$P_{fe} = m_{fe}(k_{hy}fB_{fe} + k_{ex}f^{1.5}B_{fe}^2e + k_{ec}f^2B_{fe}^2) \qquad (2)$$
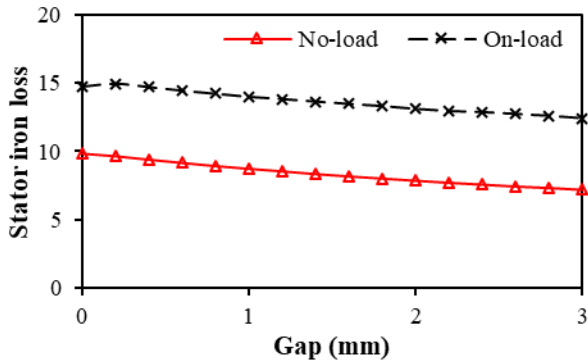
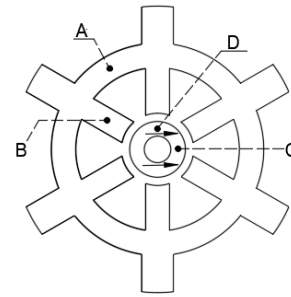**FIGURE 25.** Comparison of stator iron losses under no-load and on-load condition with variation of stator gap.

FIGURE 27. Point A (middle of yoke), B (middle of tooth), C (middle of North pole), D (middle between north and south poles).
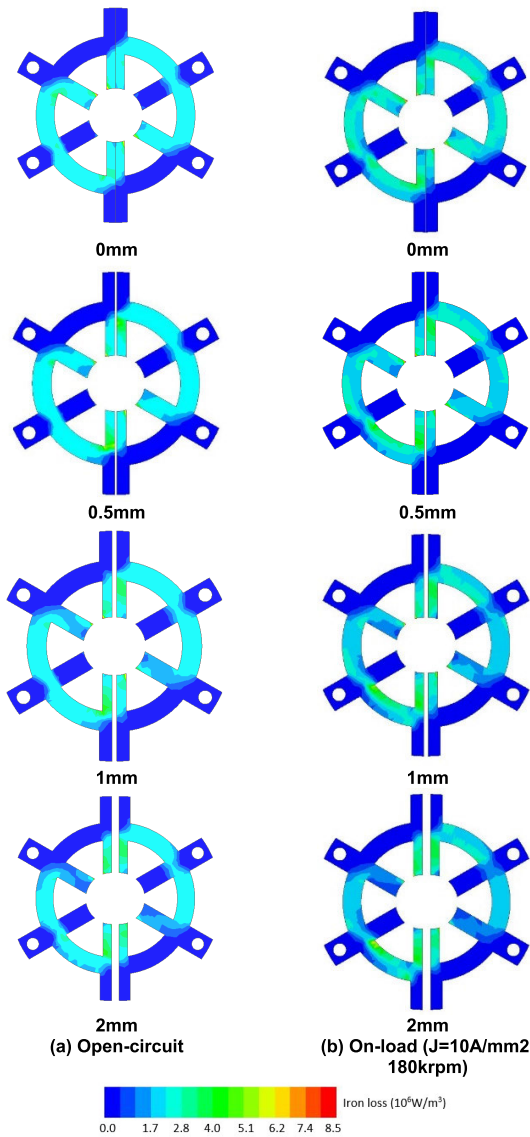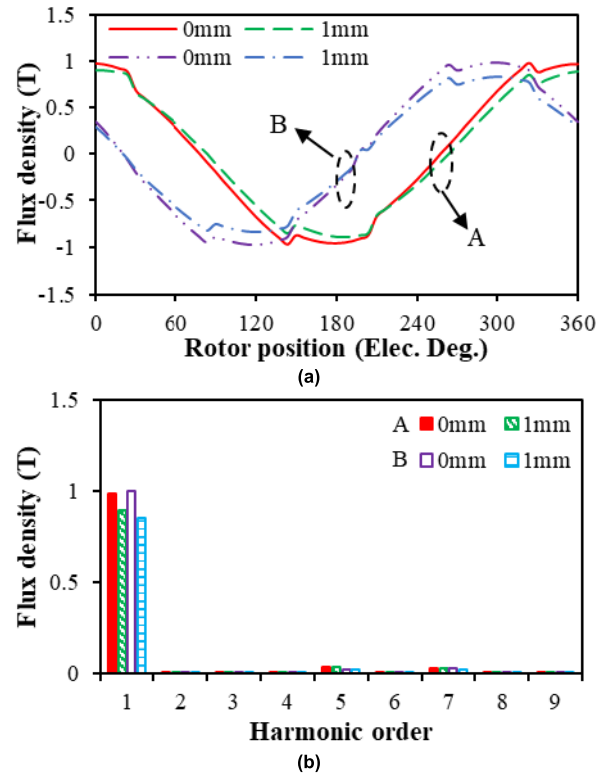

(a)

(b)

FIGURE 28. Comparison of flux densities at points A and B with 1mm and without stator gap ($J = 10A/mm^2$, 180krpm). (a) Waveforms. (b) Harmonics.

(a) Open-circuit

(b) On-load (J=10A/mm2, 180krpm)

Iron loss (10⁶W/m³)

0.0   1.7   2.8   4.0   5.1   6.2   7.4   8.5

FIGURE 26. Stator iron loss distributions with different stator gap.

where m_{fe} is the stator mass, k_{hy}, k_{ex} and k_{ec} are the hysteresis coefficient, eddy current coefficient and excess loss coefficient respectively. f denotes the fundamental frequency and B_{fe} represents the peak value of the stator iron flux density.

Fig. 25 compares the no-load and on-load stator iron losses of the motors with different stator gaps. It can be seem that the no-load and on-load stator iron losses all decrease with the increase of gap, and the on-load stator iron loss is larger than no-load stator iron loss for each gap. Therefore, the influence of armature reaction on the stator iron loss cannot be neglected.

Fig. 26 shows the stator iron loss distributions of the motors with different gaps. It can be clearly observed that the stator iron losses in the split stator teeth are increased and in other parts are decreased with stator gap. For further investigation, by way of example as shown in Fig. 27, point A is chosen in the middle of yoke between two teeth, and point B is chosen
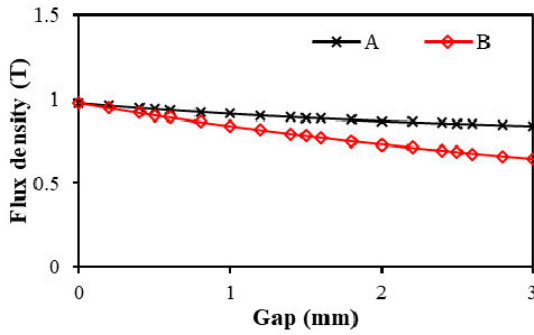
FIGURE 29. Variation of fundamental value of stator flux density of the motor with 1mm and without stator gap (J = 10A/mm^2, 180krpm).
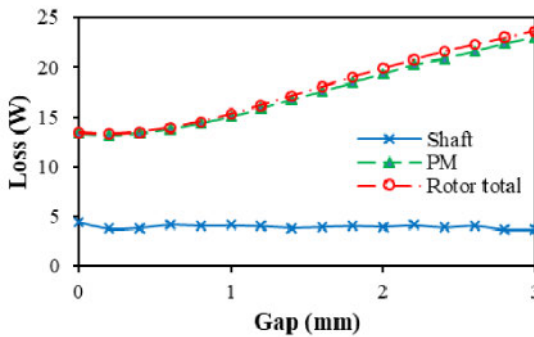

FIGURE 30. Loss of the motor with different stator gaps (J = 10A/mm^2, 180krpm).

in the middle of the tooth to compare the variation of stator iron flux density with different gaps [24].

The flux densities of points A and B of the motors with 0mm and 1mm stator gaps are compared under on-load condition, as shown in Fig. 28. It can be seen that compared with 0mm stator gap, the points A and B of the motor with 1mm stator gap have smaller amplitudes of fundamental flux densities. The amplitudes of fundamental flux density of points A and B decrease linearly when the stator gap increases, Fig. 29, which results in the decreased stator iron loss.

2) ROTOR LOSS

The effect of stator gap mainly reflects on the non-uniformed air-gap. This will result in more harmonics of air-gap flux density. The variation of shaft and PM eddy current losses, in addition the variation of rotor total loss with the gap is shown in Fig. 30. Due to the shielding effect of PM, the shaft loss is negligible. Fig. 31 shows the rotor loss distributions of the motors with different stator gaps, including magnet ring and shaft. The eddy current loss of the magnet ring increases when the stator gap increased. The shaft of this motor employs magnetic material, i.e. SUS430.

In order to verify that the increase of magnet eddy current loss is due to the increase of spatial harmonics, the on-load air-gap flux density distributions of the motors with 0mm and 1mm stator gap are shown in Fig. 32. The variation of each harmonic is shown in Fig. 33. Under on-load condition,
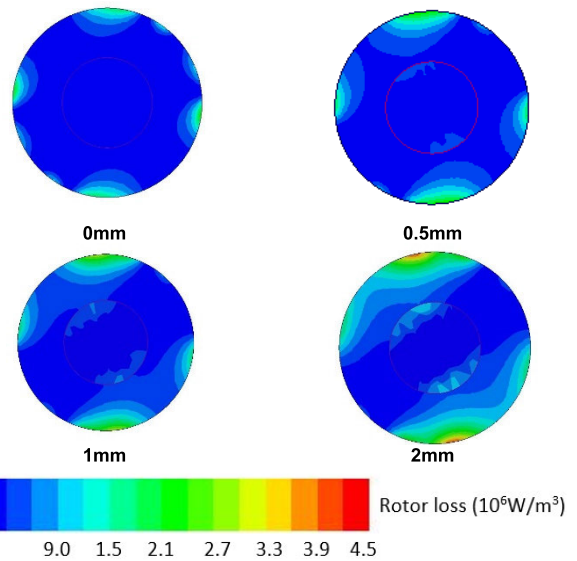

FIGURE 31. Rotor loss distributions with different stator gap (J = 10A/mm^2, 180krpm).
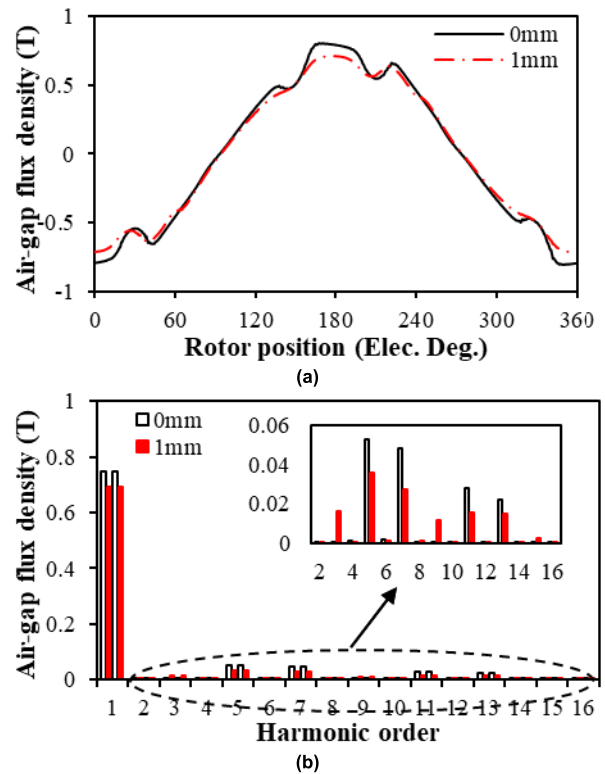

FIGURE 32. Air-gap flux densities of the motor with 1mm stator gap and no stator gap (J = 10A/mm^2, 180krpm). (a) Waveforms. (b) Harmonics.

with the increased stator gap, the 3rd and 9th harmonics are appeared and increased, while the 5th and 7th harmonics are decreased.

For further investigation, Fig. 34 shows the variation of magnet eddy current loss due to armature reaction only and

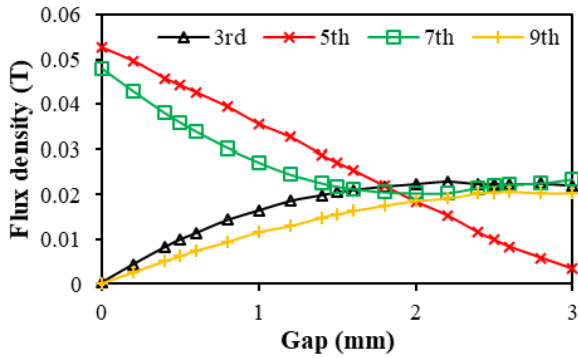**FIGURE 33.** Variation of harmonics of air-gap flux density with stator gap (J = 10A/mm^2, 180krpm).
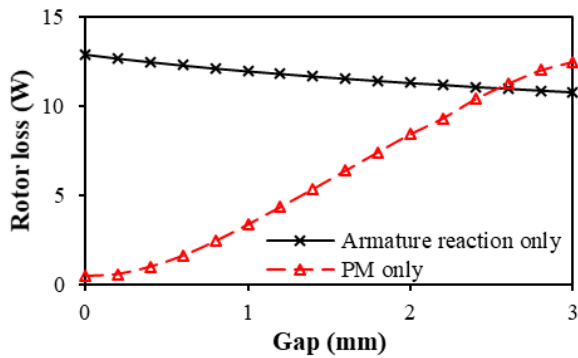

FIGURE 34. Variation of rotor total loss due to PM only and armature reaction only (J = 10A/mm^2, 180krpm).
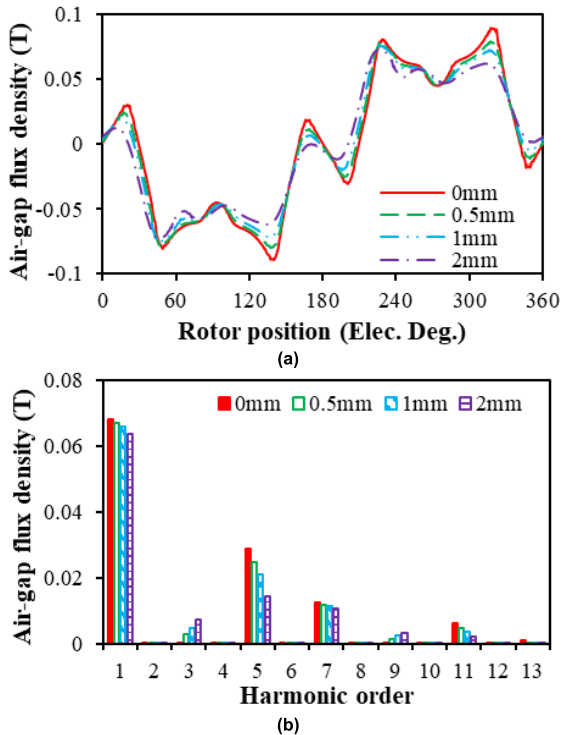

FIGURE 35. Air-gap flux density due to armature reaction only (J = 10A/mm^2, 180krpm). (a) Waveforms. (b) Harmonics.

FIGURE 36. Flux density of Point C with different stator gaps under on-load condition. (a) Waveforms. (b) Harmonics.

FIGURE 37. Flux density of Point C with different stator gaps under no-load condition. (a) Waveforms. (b) Harmonics.

PM only with stator gap. It can be seen that the rotor PM loss due to armature reaction only is significantly larger than that due to PM only. In addition, with the increase of
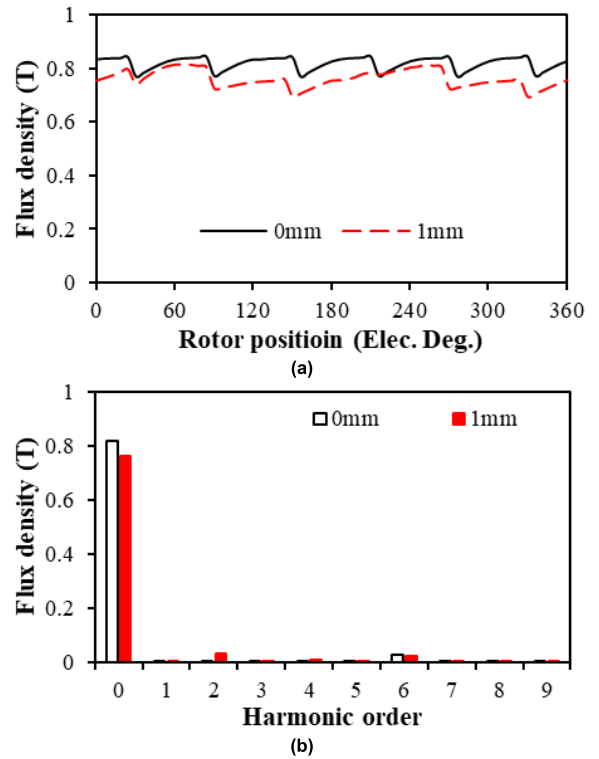
stator gap, the rotor PM loss due to armature reaction only decreases, but that due to PM only increases significantly. Fig. 35 shows the influence of stator gap on the air-gap field

FIGURE 38. Flux density of Point D with different stator gaps under on-load condition. (a) Waveforms. (b) Harmonics.
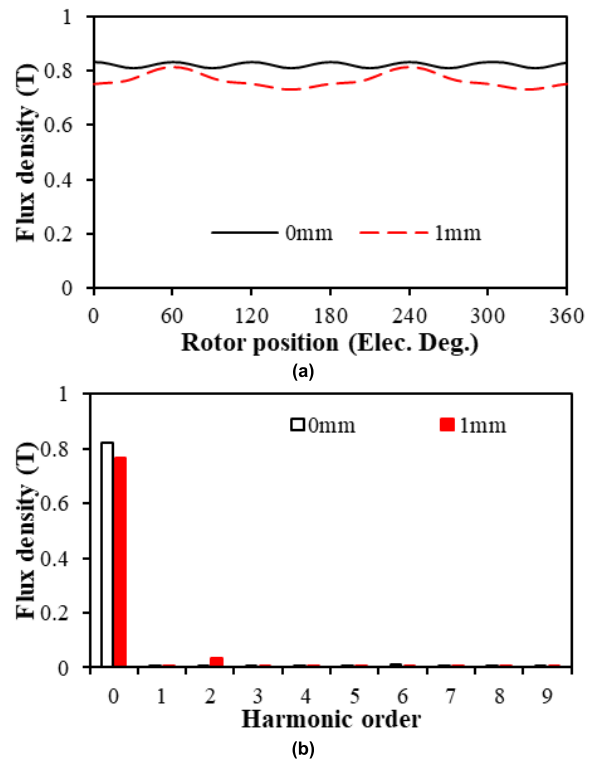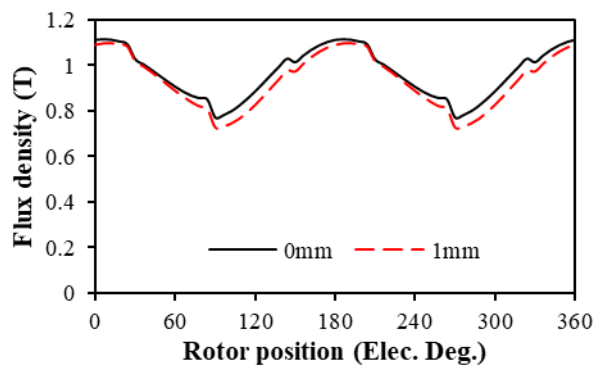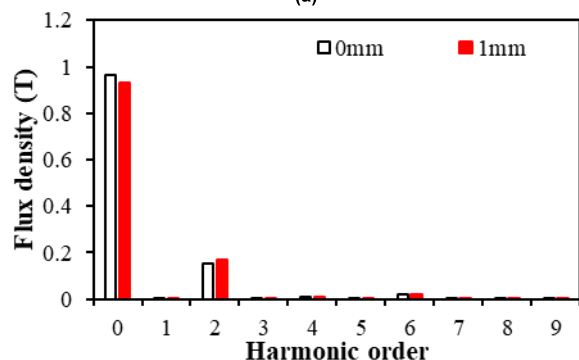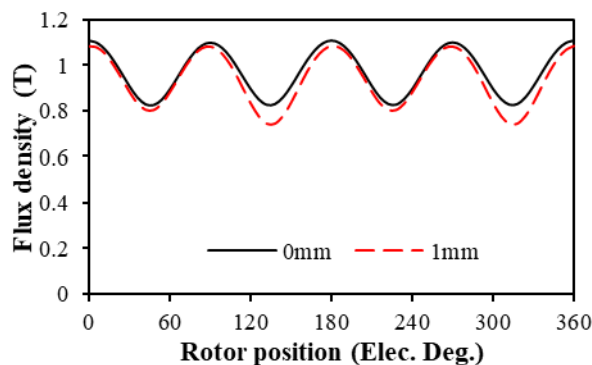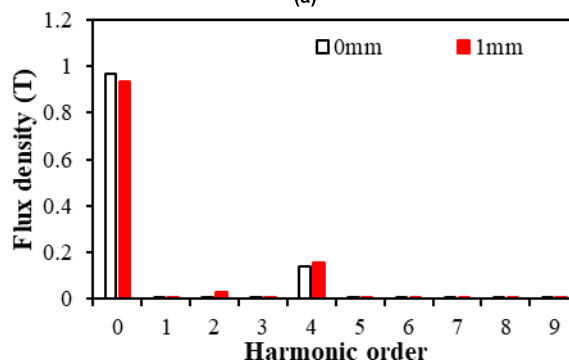

FIGURE 39. Flux density of Point D with different stator gaps under no-load condition. (a) Waveforms. (b) Harmonics.

due to armature reaction only. It shows that the stator gap decreases the amplitudes of fundamental, 5th, 7th, and 11th order harmonics caused by armature reaction. Fig. 12 shows the influence of stator gap on the air-gap field due to PM only.

Since the PM eddy current loss has direct relationship with the flux density produced by the magnet, the influence of stator gap on the flux density of magnet will be investigated in this part. Point C is chosen in the middle of north pole and point D is chosen in the middle between south and north pole, as shown in Fig. 27. Figs. 36 and 37 compare the flux densities at point C with 0mm and 1mm stator gap under on-load and no-load conditions, respectively. The amplitude of the 2nd order harmonic increases with the increase of stator gap no matter what is the condition, which results in the increase of the PM eddy current loss. Figs. 38 and 39 show almost the same results for point D. It is worth noting that under no-load condition, the flux density of point D exists the 4th order harmonic.

V. ELECTROMAGNETIC PERFORMANCE WITH MISALIGNED STATOR STRUCTURE

Another potential manufacturing tolerance of the completed assembly is shown in Fig. 40. For simplicity, assuming one stator split part is assembled with uniform air-gap distribution but the other part is assembled with unbalanced air-gap distribution. The offset value is defined as *m* in Fig. 40. In this section, the influence of the misaligned stator structure on
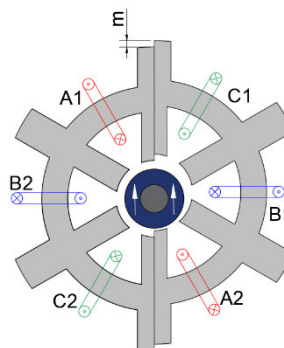

FIGURE 40. 6s/2p HSPM toroidal motor with misaligned stator structure.

the electromagnetic performance is investigated, including air-gap field, back-EMF, cogging torque, torque, and various loss components.

A. AIR-GAP FLUX DENSITY
The open-circuit equal potential distributions of motors with different offset values, i.e. 0, 0.5 and 0.7 mm are presented in Fig. 41. Fig. 42 shows that there exists a pulsation in the air-gap flux density waveform due to the sudden change of the equivalent air-gap, and the magnitude of pulsation increases with the increase of offset value. The spectra show that the misaligned assembly leads to the 2nd, 3rd, and 4th order harmonics of air-gap flux density, and the magnitudes
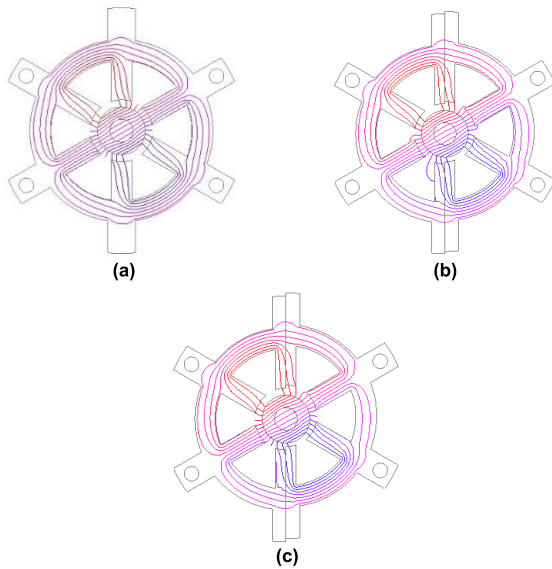
FIGURE 41. Equal potential distributions of motors with misaligned assembly. (a) No offset. (b) m = 0.5mm. (c) m = 0.7mm.
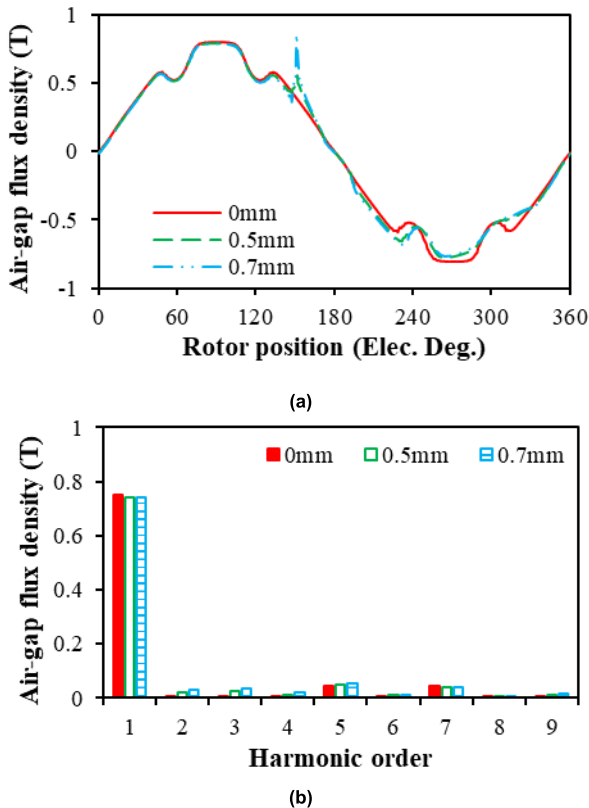

FIGURE 42. Air-gap flux density distributions of the motor with different offset values on circular path away from rotor by 0.775 mm. (a) Waveforms. (b) Harmonics.

of those additional harmonicas increase with the increased offset value. However, the misaligned assembly has almost no influence on the fundamental amplitude of air-gap flux density.
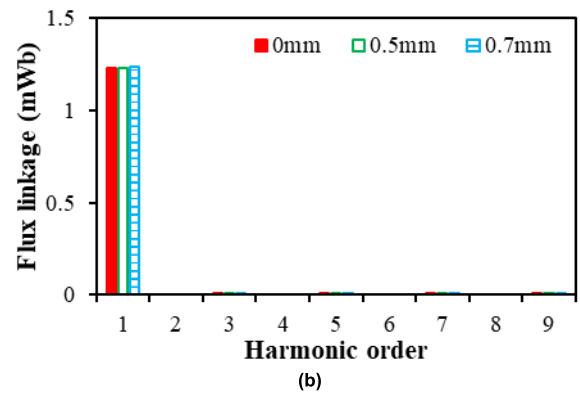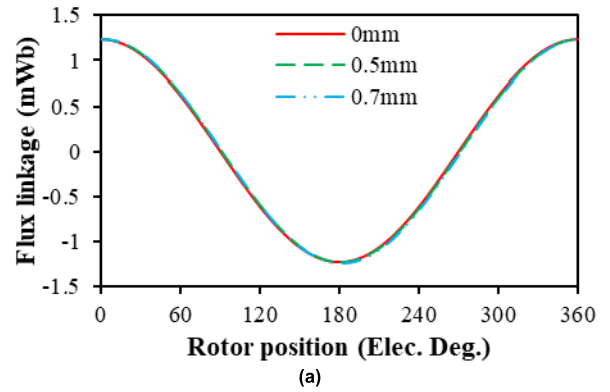

FIGURE 43. Flux linkage of phase A with different offset values. (a) Waveforms. (b) Harmonics.
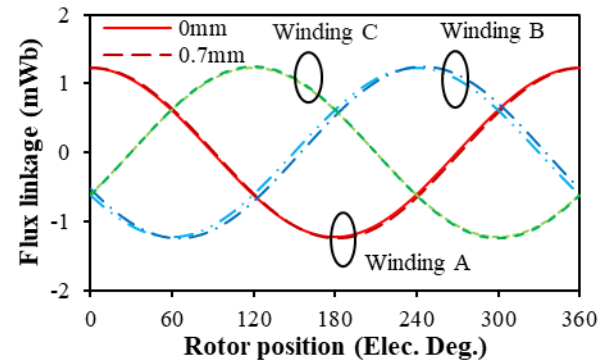
FIGURE 44. Flux linkage waveforms of motor with 0 and 0.7mm offset values.

B. FLUX LINKAGE

Fig. 43 shows the influence of misaligned assembly on the flux linkage. In terms of phase angle, phase B is retarded, and the offset phase angle of the flux linkage in phase B increases with the increase of offset value. The variation of winding B1 has the biggest change, Fig. 44. This is because of the asymmetric position of phase B. Besides, phase A and phase C have not much influence as Phase B.

C. BACK-EMF

Fig. 47 shows that the increased misaligned offset value has almost no effect on the amplitude of fundamental back-EMF

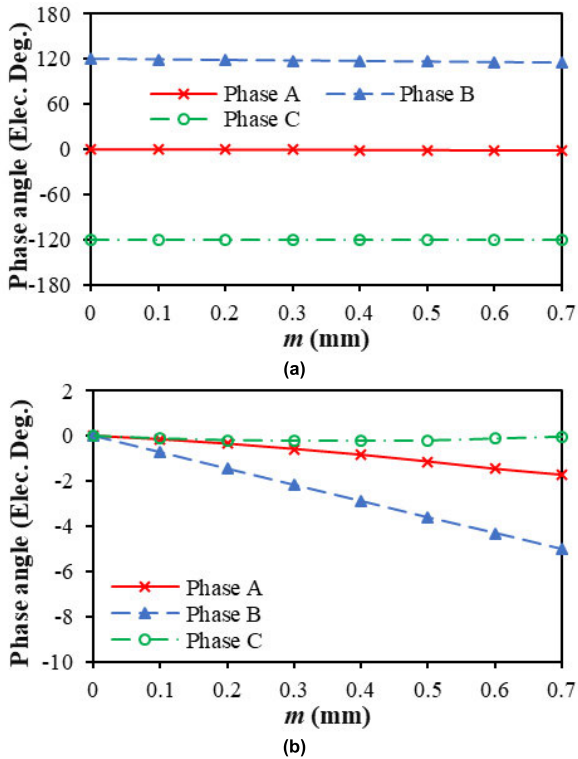**FIGURE 45.** Influence of misaligned offset value on phase angle of flux linkage. (a) Phase angle. (b) Offset phase angle.
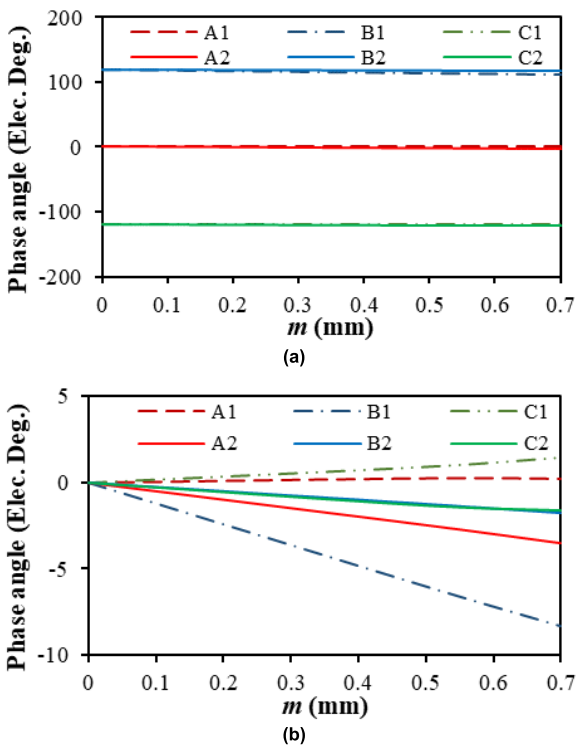
FIGURE 46. Influence of misaligned offset value on winding angle of flux linkage. (a) Phase angle. (b) Offset phase angle.
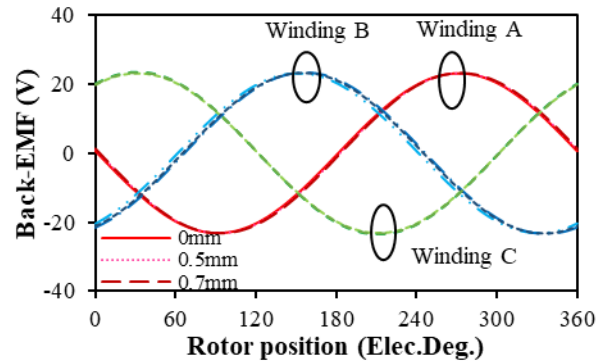
FIGURE 47. Back EMF waveforms of motors with different offset values.
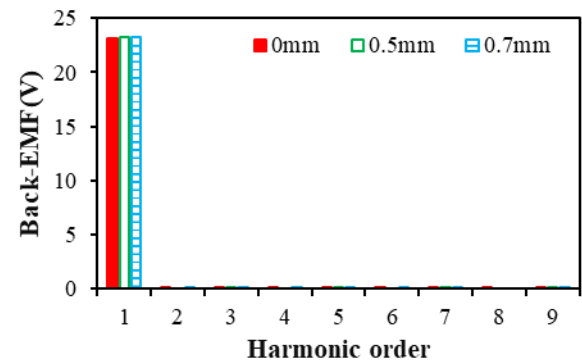
FIGURE 48. Back EMF harmonics of Phase A with different offset values.
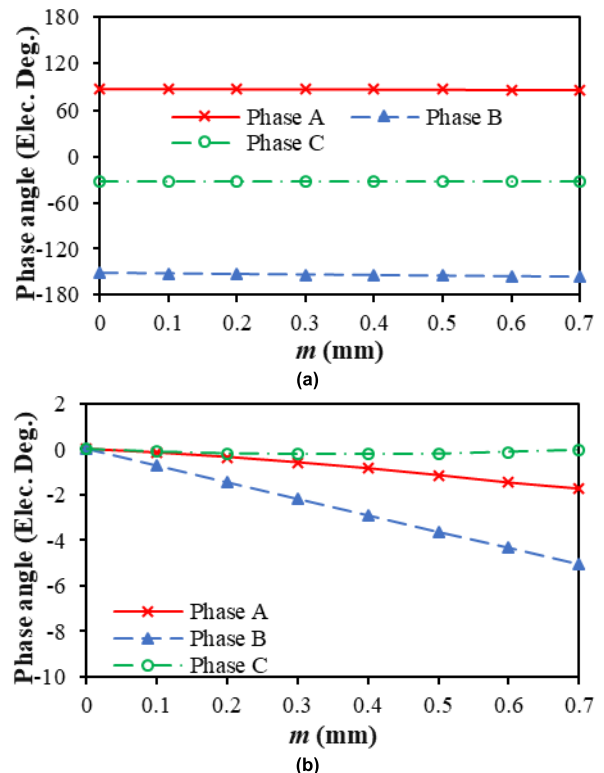
FIGURE 49. Influence of misaligned offset value on phase angle of back EMF. (a) Phase angle. (b) Offset phase angle.

and does not change the harmonic contents. With the same result of flux linkage, the misaligned offset value affects the phase angle of three phase back-EMFs, which leads to the unbalanced three phase back-EMFs. Fig. 49 shows the variation of the phase angles and offset phase angles of three phase back-EMFs with misaligned offset value. It can be seen

FIGURE 50. Cogging torque of the motors with different misaligned offset value. (a) Waveforms. (b) Harmonics.

FIGURE 51. Influence of misaligned offset values on peak cogging torque.

FIGURE 52. Torque of motors with different misaligned offset value (J = 10A/mm^2). (a) Waveforms. (b) Harmonics.
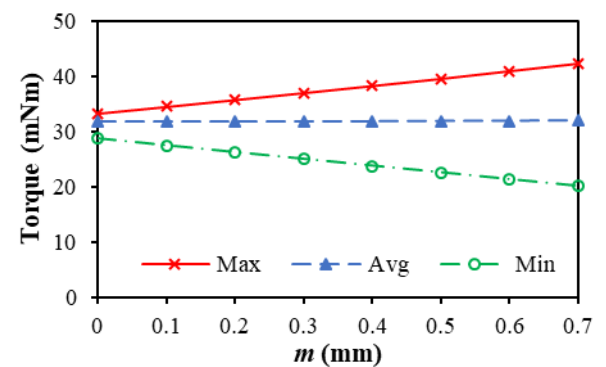
FIGURE 53. Influence of misaligned offset value on output torque.

that the offset phase angles of phase A and Phase B increases with the offset value, but phase C remains the same. Since the misaligned assembly is located between phase A and phase C, phase B suffers most serious asymmetric and thus has the largest offset phase angle.
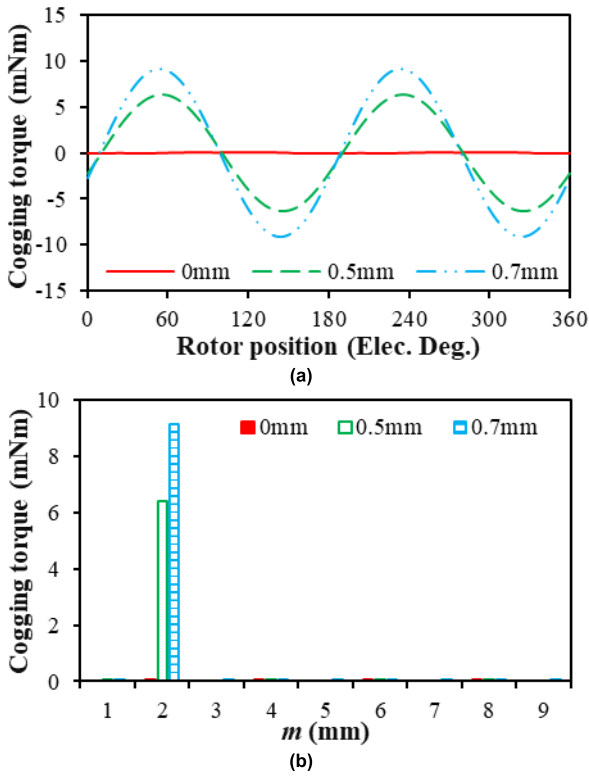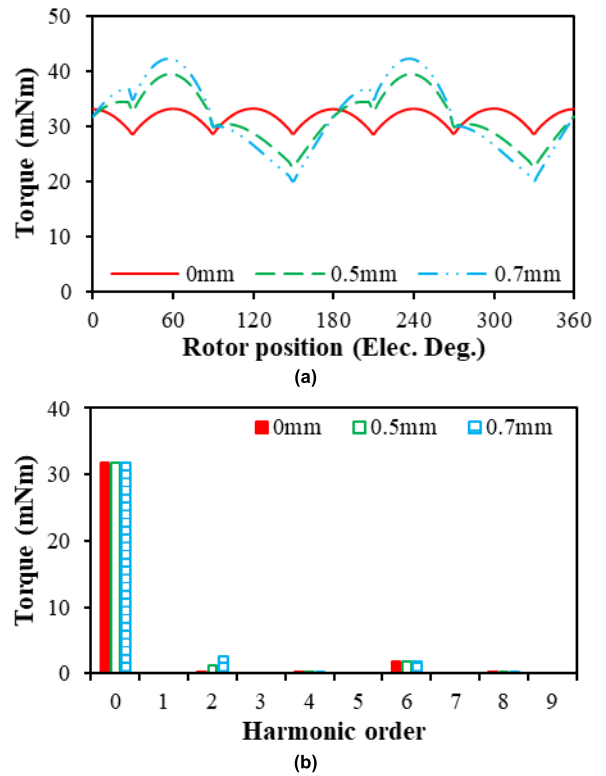
D. COGGING TORQUE

Generally, the 6s/2p PM motor with diametrically-magnetized magnet has negligible cogging torque. Significant cogging torque is produced due to the misaligned assembly. Figs. 50 and 51 show that the peak cogging torque rises with the increase of misaligned offset values.

E. ELECTROMAGNETIC TORQUE

The influence of different misaligned offset values on the electromagnetic torque is shown in Fig. 52. It can be seen that the torque ripples rise with the increase of the misaligned offset value due to the increase of peak cogging torque. The spectra show that the misaligned assembly does not change the magnitudes of the fundamental and the 6th order harmonic, but leads to the 2nd order harmonic, which results from the cogging torque. It is assumed that the influence of on-load condition on cogging torque is neglected. Fig. 53 shows that the misaligned assembly has negligible influence on the average torque.

FIGURE 54. Inductances of the motors with different misaligned offset values. (a) Self-inductance. (b) Mutual-inductance.

FIGURE 55. Variation of various loss components of the motors with different misaligned offset values ($J = 10A/mm^2$, 180krpm).
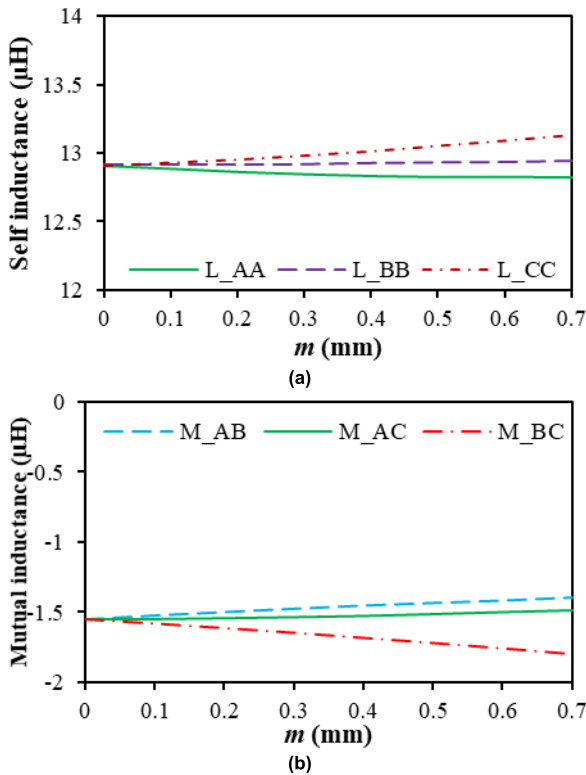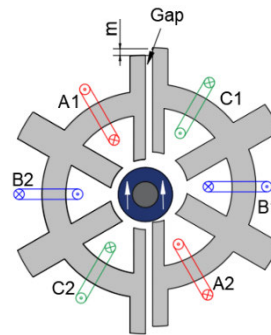

FIGURE 56. 6s/2p HSPM toroidal motors with stator gap and misaligned assembly.
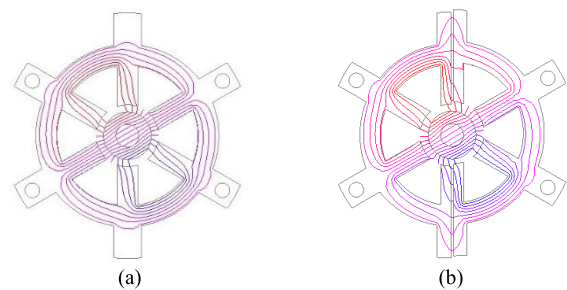
FIGURE 57. Equal potential distributions of 6s/2p HSPM toroidal motors. (a) Gap = 0mm, m = 0mm. (b) Gap = 0.5mm, m = 0.5mm.

F. INDUCTANCE

High speed motors normally have small winding inductances. Even though there is a slight change of inductance due to the stator gap, the influence could be significant. The inductance is calculated by FEA, when only one phase excited (Ia = 1A, Ib = 0A, Ic = 0A). Fig. 54 shows that the influence of misaligned assembly has negligible influence on the self- and mutual- inductances.

G. LOSS

As mentioned before, the gap between the stator segments affects the stator iron loss due to the spatial harmonics in MMF. The misaligned assembly has negligible influence on MMF, and thus the stator iron loss remains unchanged with the offset values, Fig.55. In this part, the ac effect on the copper loss is again neglected. Thus, only dc copper loss is considered and it remains unchanged with the misaligned offset value. Misaligned assembly leads to non-uniformed air-gap and thus increases the rotor PM loss, as shown in Fig. 55. In summary, with the increase of misaligned offset value, the total motor losses increase due to the increased rotor PM loss.

VI. INFLUENCE OF BOTH GAP AND MISALIGNMENT

Fig. 56 shows the cross-sections of 6s/2p HSPM toroidally-wound motors with stator gap and misaligned assembly. The stator gap is located between the windings of phase A and

phase C, which divides the stator into two halves. The misaligned assembly also occurs between the windings of phase A and phase C.

A. AIR-GAP FLUX DENSITY

Fig. 57 compares open-circuit equal potential distributions of motors with both gap of 0.5 mm and offset values of 0.5 mm. Fig. 58 shows that there exists a pulsation in the air-gap flux density waveform due to the sudden change of the equivalent air-gap length, and the magnitude of pulsation increases with the increase of offset value. The spectra show the misaligned assembly leads to the 2nd, 3rd, and 4th order harmonics of air-gap flux density, and the magnitudes of those additional harmonicas increase with the increased

FIGURE 58. Comparison of air-gap flux density distributions of the motor with gap = 0mm, m = 0.5mm and the motor with gap = 0.5mm, m = 0.5mm on circular path away from rotor by 0.775 mm. (a) Waveforms. (b) Harmonics.

FIGURE 59. Comparison of flux linkages of the motor with gap = 0mm, m = 0.5mm and the motor with gap = 0.5mm, m = 0.5mm. (a) Waveforms. (b) Harmonics of phase A.

offset value. However, the misaligned assembly has almost no influence on the fundamental amplitude of air-gap flux density.

FIGURE 60. Comparison of flux linkages of the motor with gap = 0mm, m = 0.5mm and the motor with gap = 0.5mm, m = 0.5mm. (a) Waveforms. (b) Harmonics of phase A.
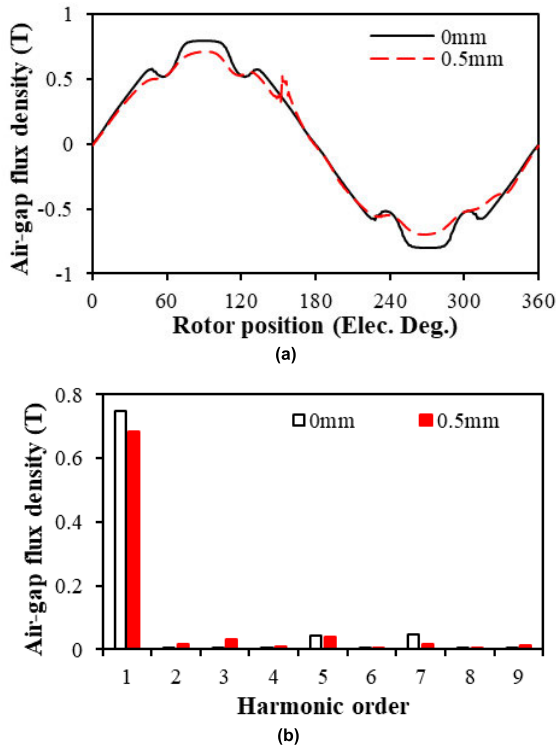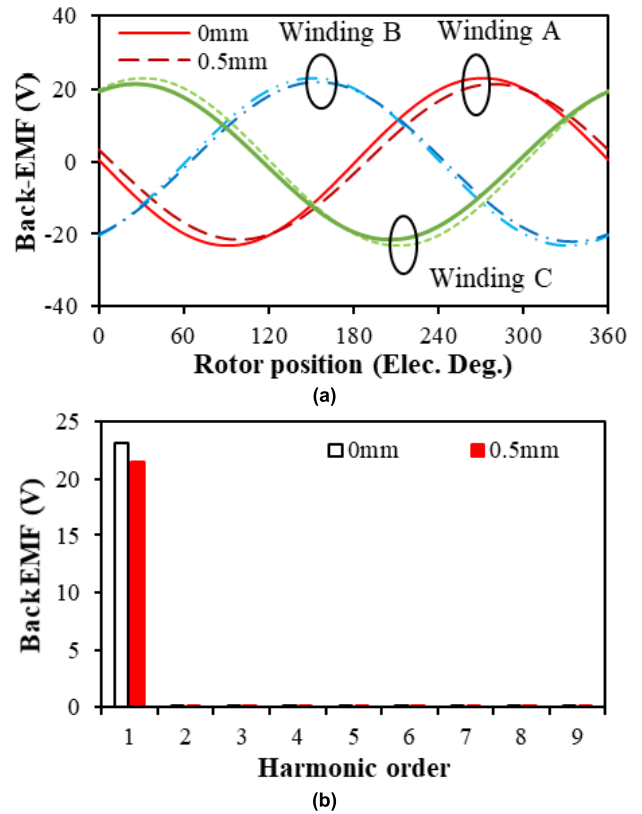
B. FLUX LINKAGE

Fig. 59 shows the influence of misaligned assembly on the flux linkage. It can be seen that misaligned mainly affect the phase angle of phase B. Gap affects both the amplitudes of fundamental and phase angles of phase A and phase C.

C. BACK-EMF

The comparison of no gap and misaligned with 0.5mm gap and misaligned off-set value is shown in Fig. 60. It can be seen that both the amplitude of fundamental back-EMF and the harmonic contents changed. With the same result of flux linkage, the misaligned offset value affects the phase angles of three phase back-EMFs, which leads to the unbalanced three phase back-EMFs.

D. COGGING TORQUE

Cogging torque has been affected significantly by either gap or misalignment. Fig. 61 shows with 0.5mm gap and misaligned off-set value, cogging torque is significantly changed due to asymmetric and uniform structure.

E. ELECTROMAGNETIC TORQUE

Comparison of the motor with no gap and misalignment and the motor with 0.5mm gap length and misaligned off-set value is shown in Fig. 62. It can be seen that the torque

FIGURE 61. Comparison of cogging torques of the motor with gap = 0mm, m = 0.5mm and the motor with gap = 0.5mm, m = 0.5mm. (a) Waveforms. (b) Harmonics.
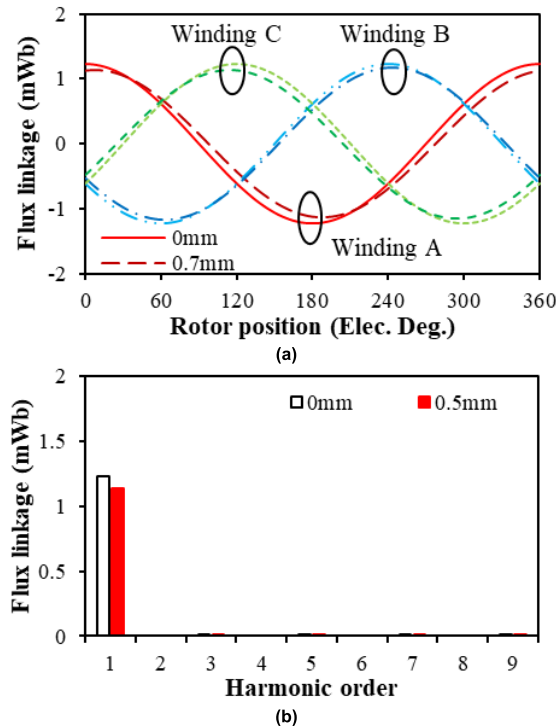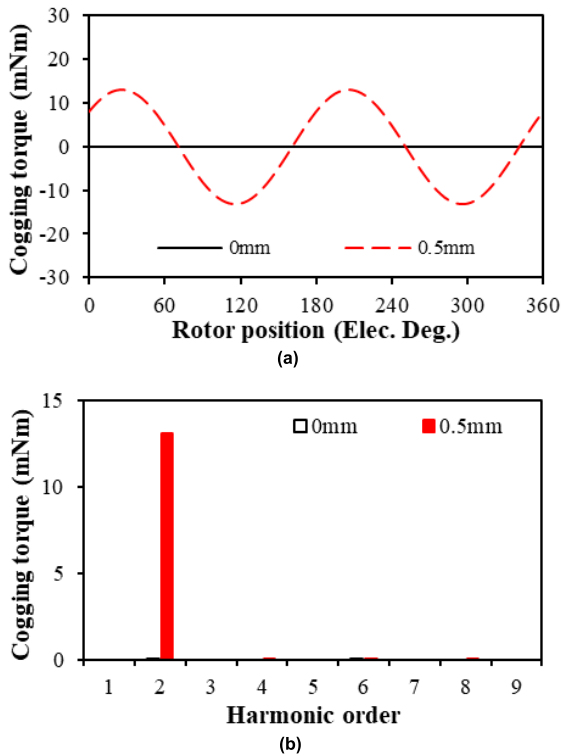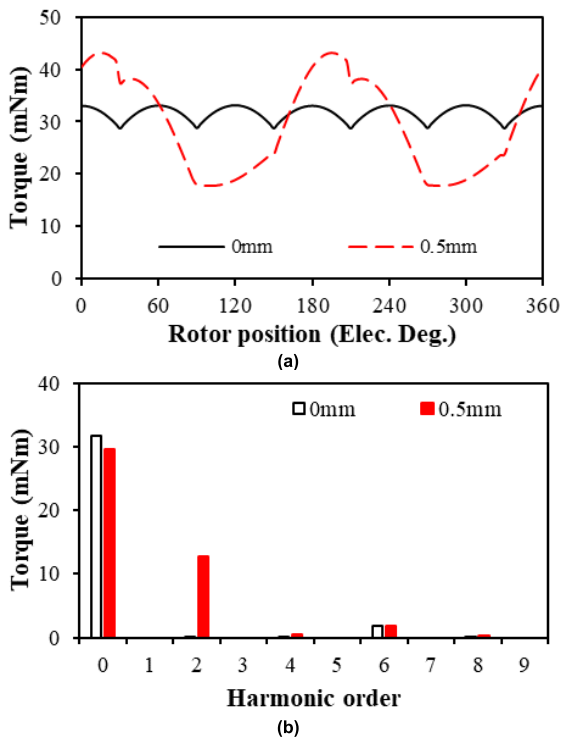

FIGURE 62. Comparison of on-load torques of the motor with gap = 0mm, m = 0.5mm and the motor with gap = 0.5mm, m = 0.5mm (J = 10A/mm^2). (a) Waveforms. (b) Harmonics.

ripples rise when the misaligned offset value increases due to the increase of peak cogging torque. The spectra show that the misaligned assembly does not change the magnitudes
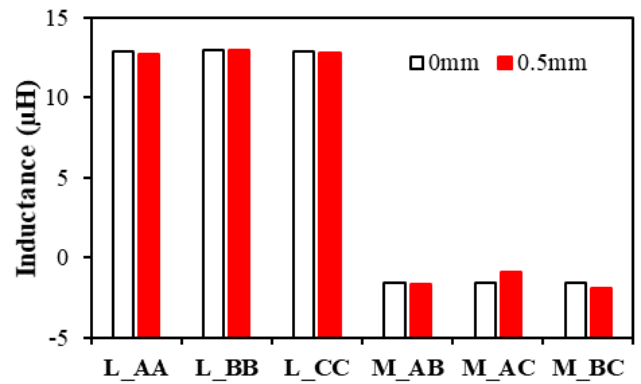
FIGURE 63. Comparison of inductances of the motor with gap = 0mm, m = 0.5mm and the motor with gap = 0.5mm, m = 0.5mm.
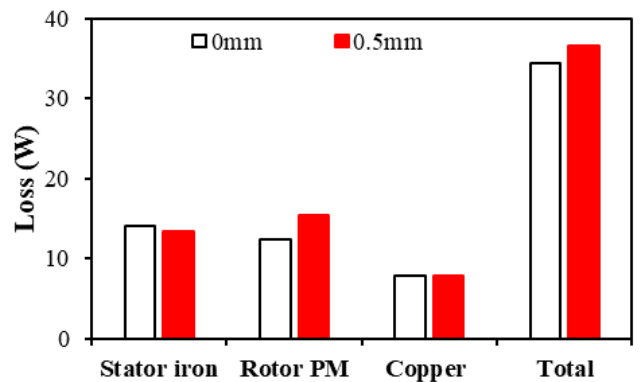
FIGURE 64. Comparison of losses of the motor with gap = 0mm, m = 0.5mm and motor with gap = 0.5mm, m = 0.5mm.

of the fundamental and the 6th order harmonic, but leads to the 2nd order harmonic, which is resulted from the cogging torque.

F. INDUCTANCE
The inductance is calculated by FEA when only one phase excited (I_a = 1A, I_b = 0A, I_c = 0A). Fig. 63 shows that the influence of misaligned assembly has negligible influence on the self- and mutual- inductances.

G. LOSS
As mentioned in section IV, the gap between the stator segments affects the stator iron loss due to spatial harmonics in MMF. The misaligned assembly has negligible influence on MMF, and thus the stator iron loss remains unchanged when the offset values increases, in Fig. 55. In this part, the ac effect on the copper loss is again neglected. Thus, only dc copper loss is considered and it remains unchanged with either the gap or the misaligned offset value. Misaligned assembly leads to non-uniformed air-gap and thus increases the rotor PM loss, as shown in Fig. 55. In summary, compared with the motor without gap and misalignment, the stator iron loss is reduced, the rotor PM loss is increased, and total loss is increased.
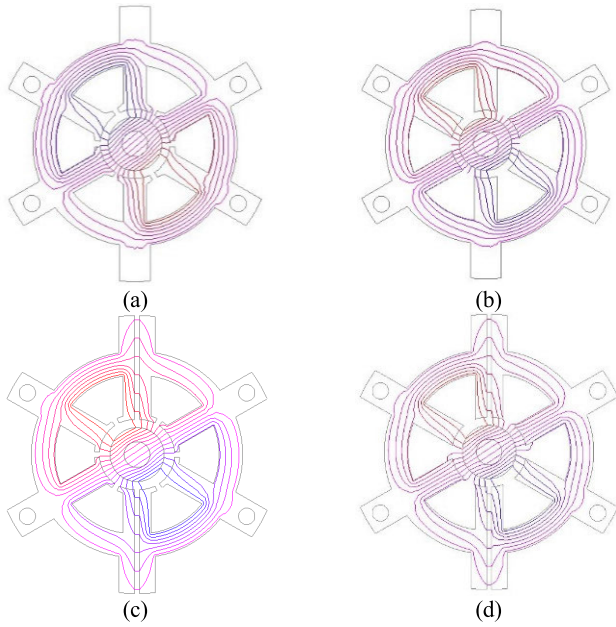
FIGURE 65. Equal potential distributions of 6s/2p HSPM toroidal motors. (a) Gap = 0mm with tooth tip. (b) Gap = 0mm without tooth tip. (c) Gap = 1mm with tooth tip and 1mm gap. (d) Gap = 1mm without tooth tip and 1mm gap.

FIGURE 66. Comparison of air-gap flux density distributions of the motor with gap = 0mm and gap = 1mm with and without tooth tip (TT) on circular path away from rotor by 0.775 mm. (a) Waveforms. (b) Harmonics.

VII. INFLUENCE OF TOOTH TIP

The influence of tooth tip is investigated in this section. Fig. 65 shows the influence of tooth tip on the equal potential

FIGURE 67. Flux linkage of motor with gap = 0mm and gap = 1mm with and without tooth tip (TT). (a) Waveforms. (b) Harmonics. (c). Phase angles.

distribution of the motor with 0mm and 1mm stator gap length. The slot opening of the motor with tooth tip is 1mm compared with 2.5mm of motor without tooth tip. Compared with motor without tooth tip, the motor with tooth tip has similar flux distribution. Fig. 66 shows the motor with tooth tip and 0mm gap has the highest fundamental amplitude and less harmonic contents of air-gap flux density than the motor without tooth tip.

Fig. 67 and Fig. 68 show the influence of tooth tip on the flux linkage and back EMF of the motor with 0mm and 1mm stator gap, respectively. It can be seen that the tooth tip has small influence on the flux linkage and back EMF. In addition, the influence of stator gap length on phase angles of
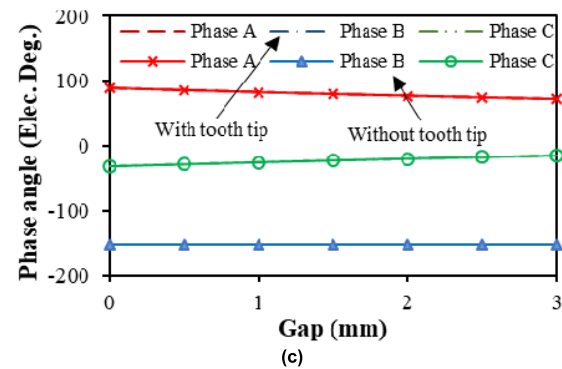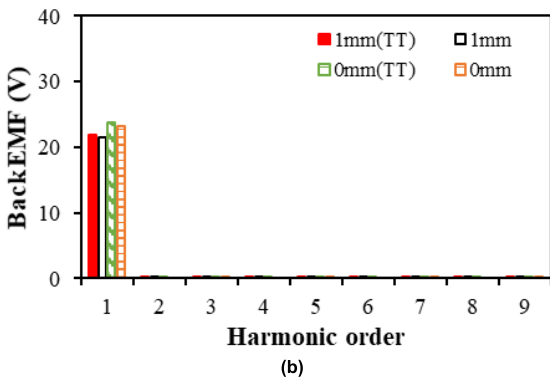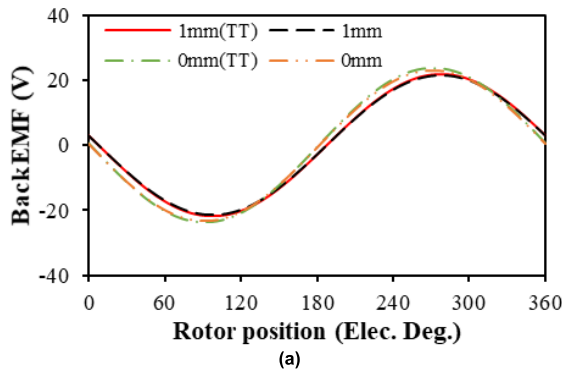
FIGURE 68. Back EMF of motor with gap = 0mm and gap = 1mm with and without tooth tip (TT). (a) Waveforms. (b) Harmonics. (c). Phase angles.
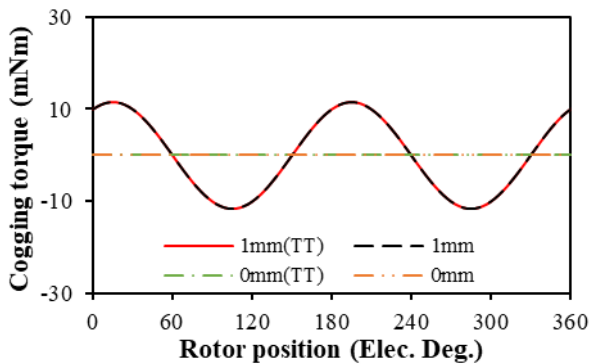
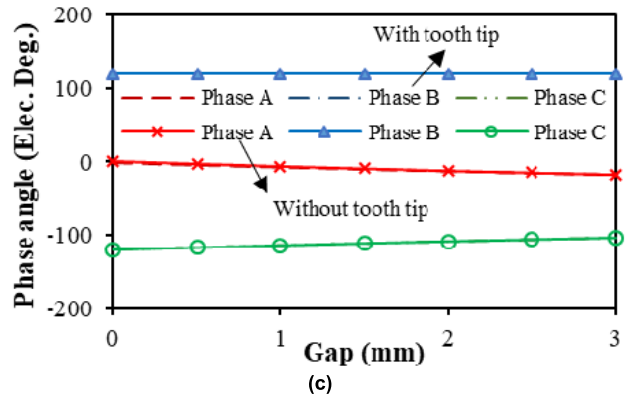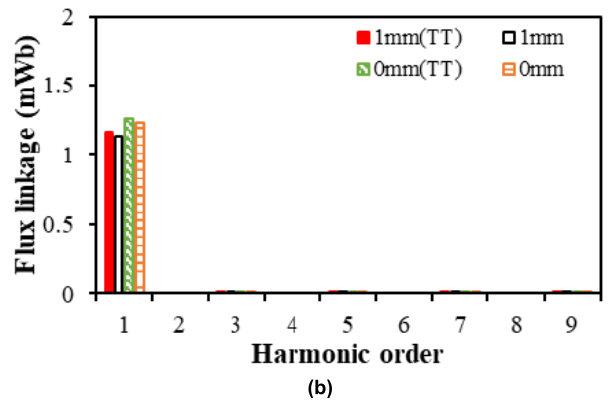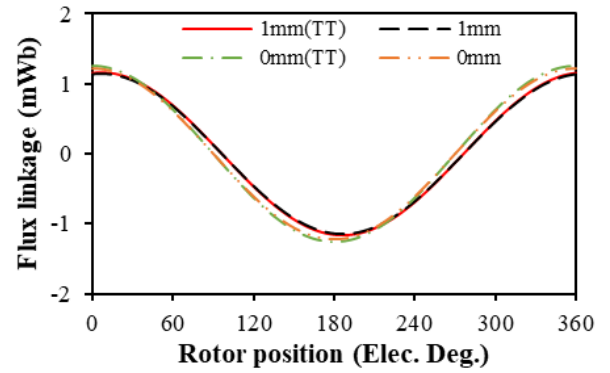**FIGURE 69.** Cogging torque of motor with gap = 0mm and gap = 1mm with and without tooth tip (TT). (a) Waveforms. (b) Harmonics. (c). Phase angles.
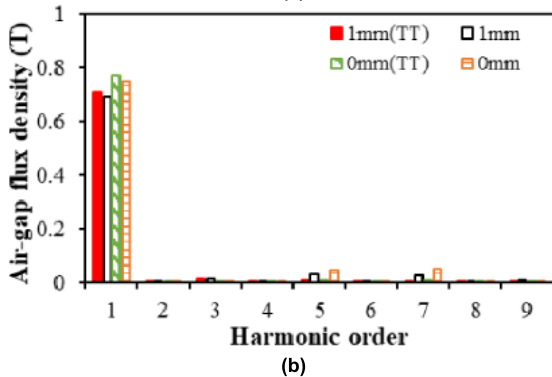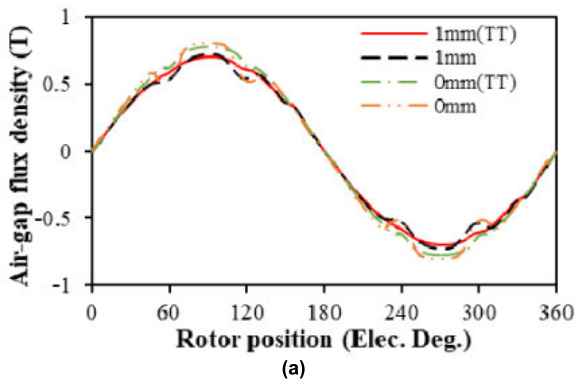

FIGURE 70. On-load torque of the motor with gap = 0mm and gap = 1mm with and without tooth tip (TT). (J = 10A/mm^2, 180krpm).
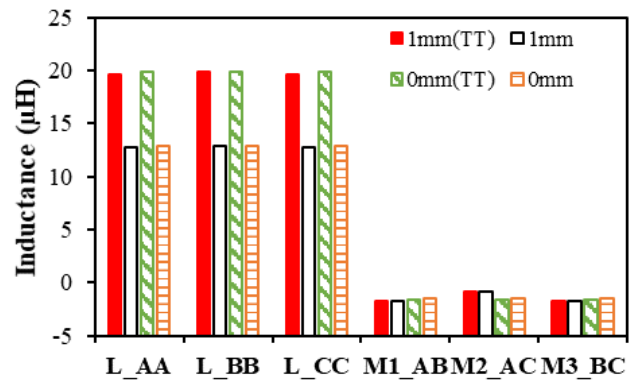
FIGURE 71. Comparison of inductances of motor with gap = 0mm and gap = 1mm with and without tooth tip (TT).
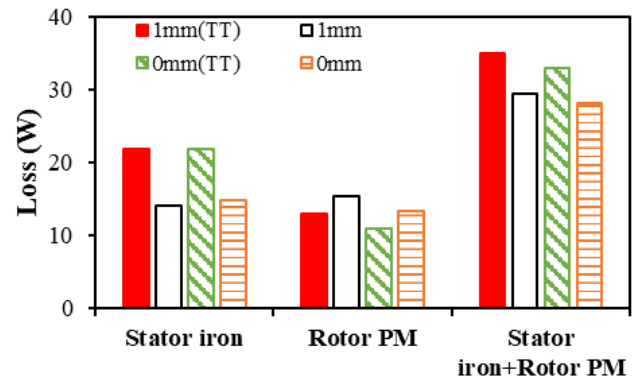
FIGURE 72. Comparison of losses of motor with gap = 0mm and gap = 1mm with and without tooth tip (TT) (J = 10A/mm^2, 180krpm).

motor with tooth tip has the same trend as the motor without tooth tip. Fig. 69 shows the cogging torque waveforms of the 0mm and 1mm stator gap motors with and without tooth tip.

It shows the tooth tip has almost no influence on the cogging torque of the motor with 1mm stator gap. Therefore, for 6s/2p HSPM motor with 1mm stator gap length, the tooth tip only affects the air-gap flux density, and it reduces the fundamental amplitude and harmonic contents.

Fig. 71 shows the influence of tooth tip on the inductance of the motor with 0mm and 1mm stator gap. The inductances are calculated by FEA. It shows that the tooth tip has large
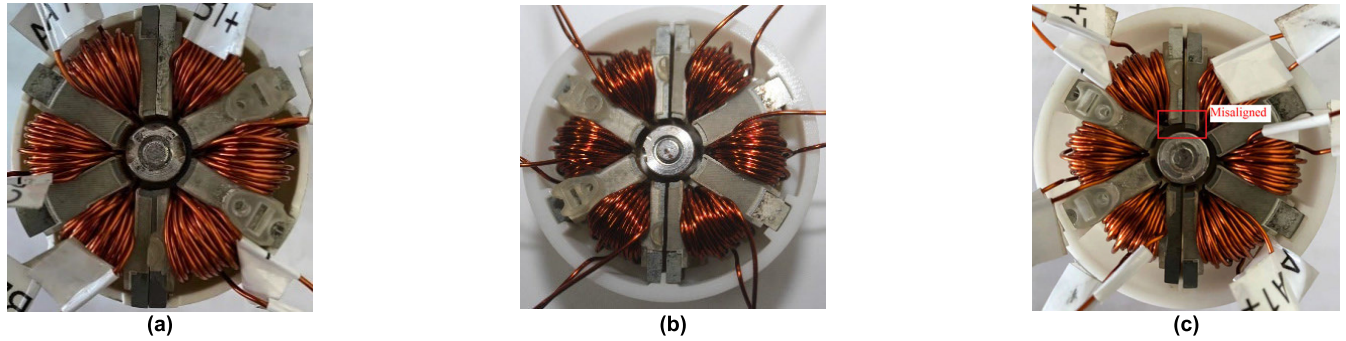
FIGURE 73. Prototypes of the 6s/2p HSPM motor. (a) No stator gap & no misalignment. (b) 1mm stator gap & no misalignment. (c) 1mm stator gap & 1mm misalignment.
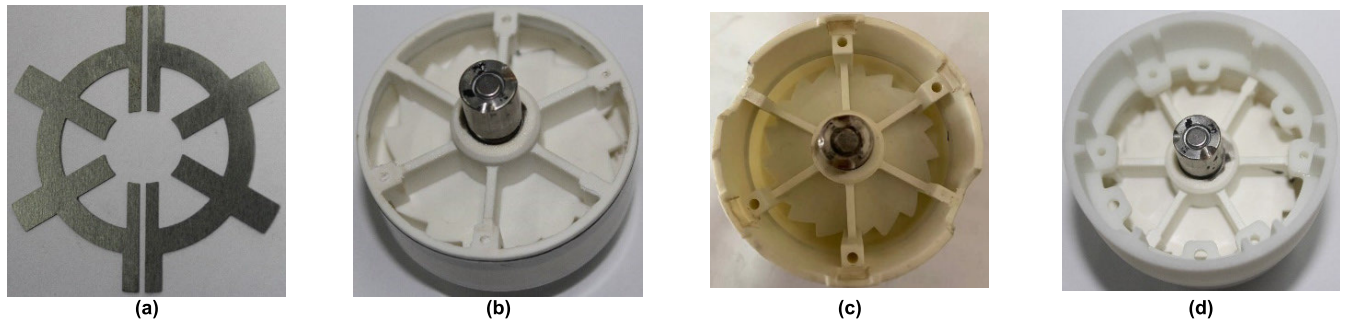
FIGURE 74. Stator lamination and frame structure. (a) Modular stator lamination. (b) Rotor-bearing system, (c) Frame structure without stator gap. (d) Frame structure with 1 mm stator gap.

influence on the self-inductance of the motor with and without stator gap. The reason is that tooth tip can increase flux leakage in the slot opening significantly.

Fig. 72 compares the loss of motor with and without tooth tip with 0mm and 1mm stator gap when the current density is 10 A/mm^2 at the speed of 180 krpm. It shows that tooth tip results in larger iron loss but lower rotor PM loss. With the increased gap, the rotor loss is decreased.

VIII. EXPERIMENTAL VALIDATION

In this section, the back-EMF and on-load static torque waveforms of 6-slot/2-slot PM motors with and without stator gap are measured to validate the FE predictions. Fig. 73 shows the prototypes of the 6s/2p HSPM motors without and with stator gap and misalignment. Fig. 74 shows the modular stator lamination structure, the rotor-bearing system, and the frame structures without and with 1mm stator gap. For supporting the modular stator structure with 1mm stator gap, a special frame is designed and manufactured by 3D printing. The frame has two teeth with 1mm thickness to form a 1mm stator gap. In addition, there are four slots to fix four outer teeth and support the stator structure, Figs. 74 (c) and (d).

A. BACK-EMF
Fig. 75 (I) shows the FE predicted and measured three phase back-EMF waveforms of 6s/2p motor with toroidal windings

TABLE 2. Winding resistances (m Ω).

ANA	Measured (0 Hz)	Measured (120Hz)	Measured (1000Hz)
24.3	25.1	25.5	36.5

having no stator gap and misalignment. It can be seen that the measured results agree well with the FE predictions. For the motor with 1mm stator gap and no misalignment, the FE predicted three phase back-EMF waveforms are slightly smaller than the measured results, Fig. 75 (II). In addition, the stator gap changes the phase angles of three phase back-EMF waveforms, Fig. 75 (II-c). Fig. 75 (III) shows that when the stator gap is 1mm and the misaligned offset is 1mm, the test results are in good agreement with FE prediction, including the fundamental magnitudes and phase angles of three phase back-EMFs. Overall, the influence of stator gap and misalignment on the back-EMF is verified by the measured results.

B. PHASE RESISTANCE AND WINDING INDUCTANCE
The phase resistance and winding inductances are measured by a LCR meter under 0 Hz, 120Hz and 1000 Hz, Table 2 and 3. Since the analytical prediction is DC resistance and neglecting the influence of frequency, the measured phase resistance by an ohmmeter is almost the same as the prediction.
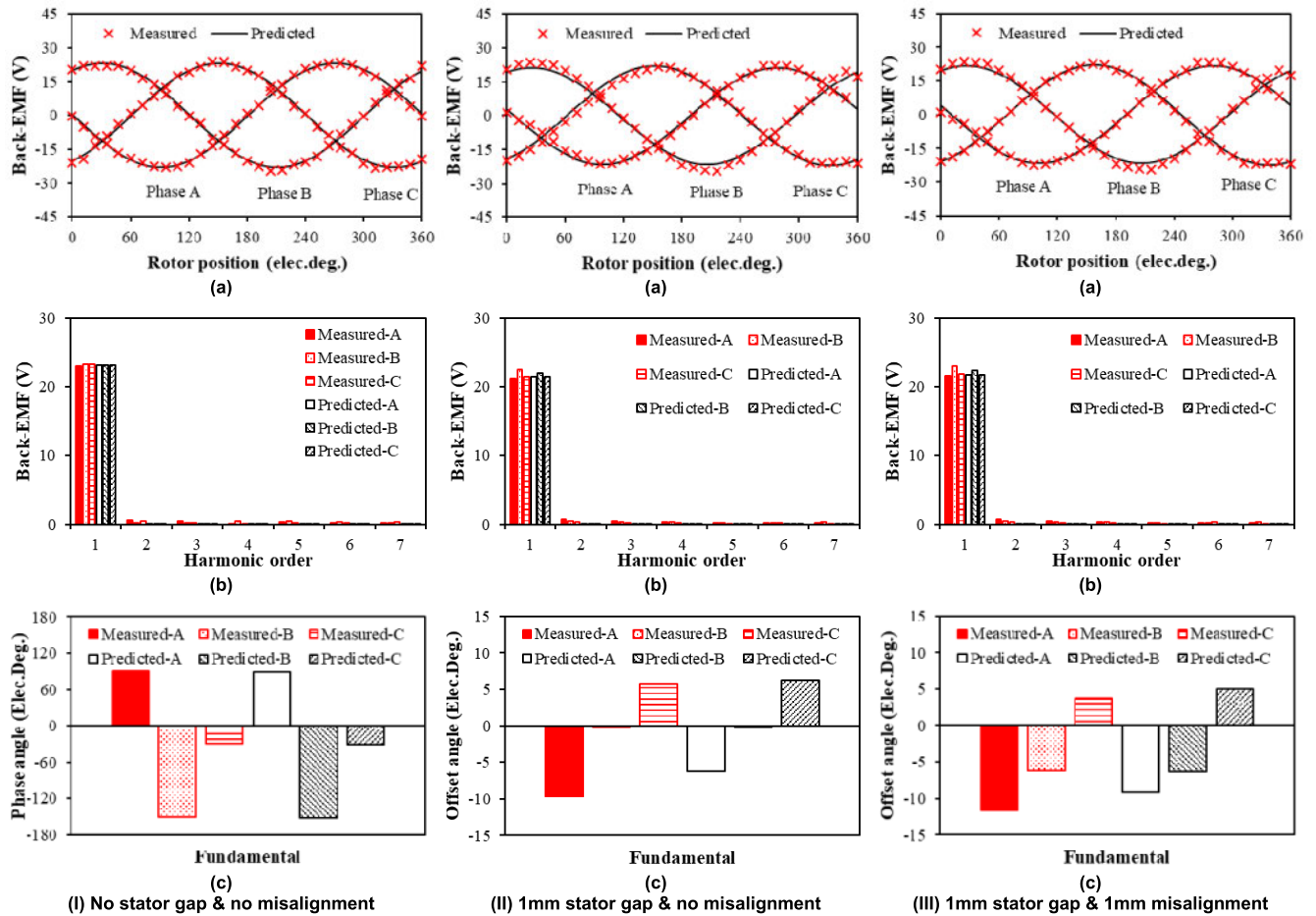
FIGURE 75. FE predicted and measured three phase back-EMF waveforms of 6s/2p motors without and with stator gap and misalignment. (a) Waveforms. (b) Spectra. (c) Phase angle.

TABLE 3. Winding inductances (μH).

		2-D FE	Measured (120Hz)	Measured (1000Hz)
No stator gap	A	14.45	24.1	23.47
	B	14.45	24.1	23.47
	C	14.45	24.1	23.47
Stator gap=1mm	A	14.50	35.93	35.40
	B	14.68	39.60	38.08
	C	14.50	35.93	35.40

Under 120Hz, the measured result is larger than the analytical result. The measured phase resistance under high frequency (1kHz) are significantly larger than that under low frequency (120Hz). For winding inductance, the FE predictions are ideal winding inductances and neglecting the influence of frequency, and thus the measured inductances are larger than the predicted results by FEA due to neglecting end-winding in 2D-FE model. With the increase of frequency, the measured inductance decreases. It is worth noting that the stator gap increases the inductance of phase B since the gap occurs between phases A and C.

C. STATIC TORQUE

In literature [20], a test rig is designed to measure the on-load static torque, Fig. 76. The cogging torque can be measured
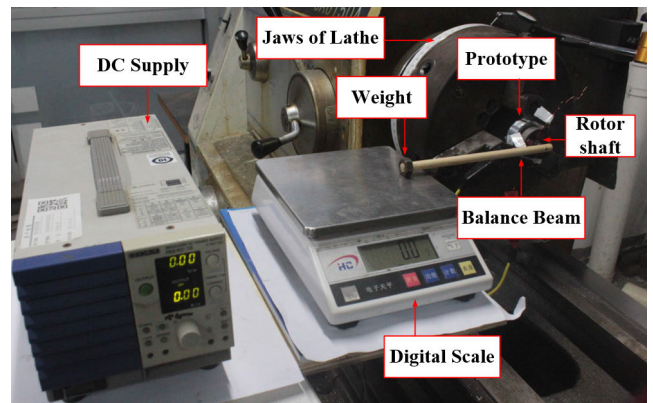
FIGURE 76. Test rig for static torque measurement.

under open-circuit condition, and with the armature currents of IA = −IB = 5A, IC = 0A, the on-load static torques of the 6s/2p motor at different rotor positions can be measured. Without and with stator gap and misalignment, the FE predicted and measured cogging torques and on-load static torques have a good agreement, Figs. 77, 78, and 79. Fig. 80 shows that with the increase of phase current,
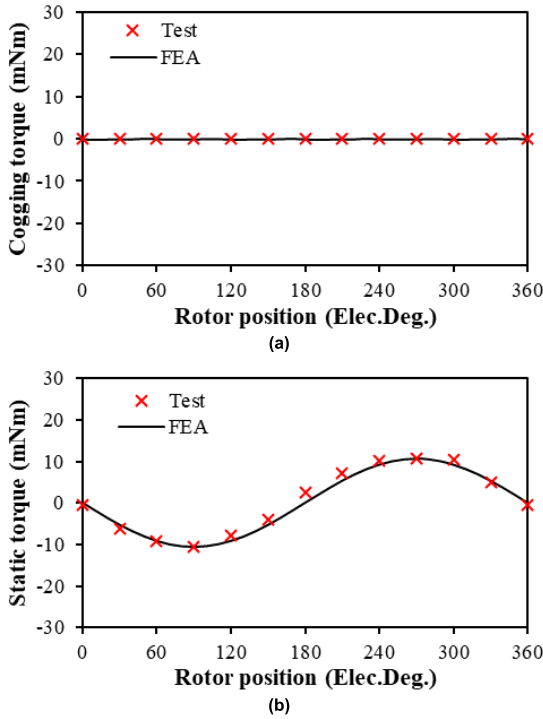
FIGURE 77. FE predicted and measured cogging torques and static torques, No stator gap, no misalignment. (a) Cogging torque. (b) Static torque.
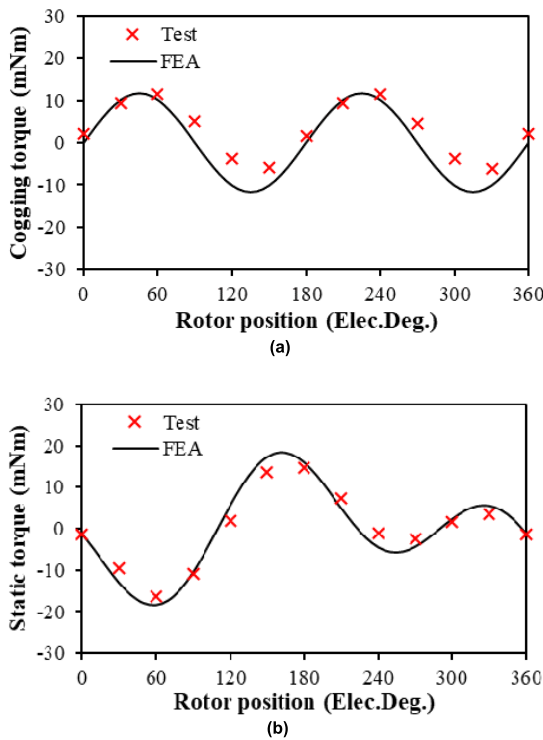
FIGURE 78. FE predicted and measured cogging torques and static torques, 1 mm stator gap and no misalignment. (a) Cogging torque. (b) Static torque.

the measured maximum static torques are in good agreement with FE predictions of 6s/2p motor without and with stator gap and misalignment
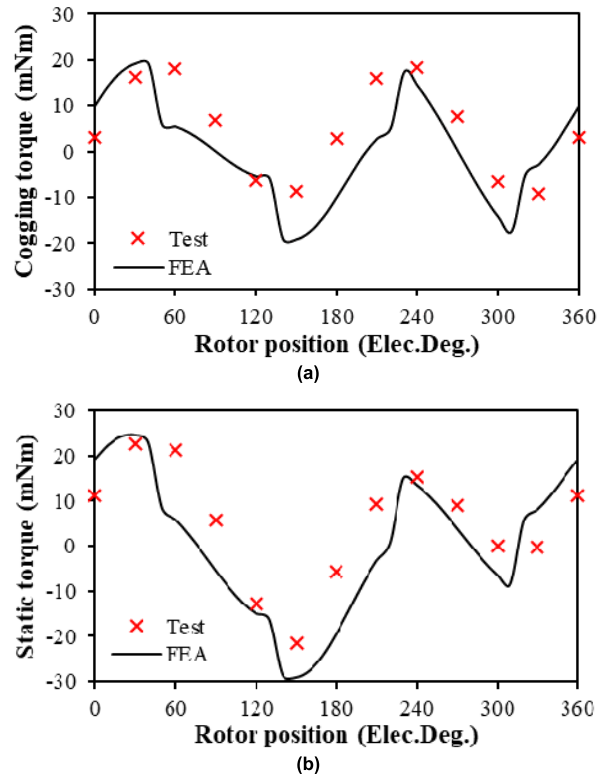
FIGURE 79. FE predicted and measured cogging torques and static torques, 1 mm stator gap and 1 mm misalignment. (a) Cogging torque. (b) Static torque.
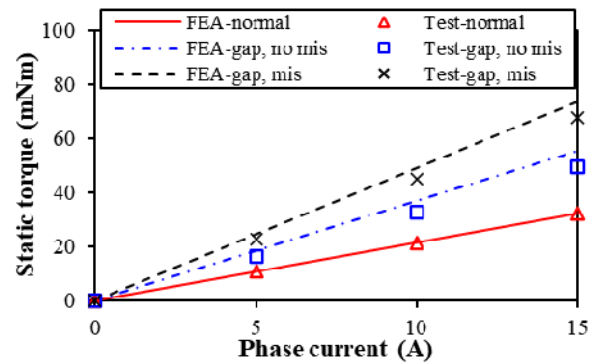
FIGURE 80. Variation of FE predicted and measured peak static torques with phase current, without and with 1 mm stator gap (gap) and 1 mm misalignment (mis).

IX. CONCLUSION

The influence of stator gap and misalignment due to manufacturing tolerances on the electromagnetic performance of 6s/2p HSPM motor with toroidal winding and diametrically magnetized PM rotor has been analyzed and experimentally validated.

It can be seen that the stator gap mainly affects the equivalent air-gap length and magnetic reluctance, which decreases the fundamental magnitude of air-gap flux density, flux linkage, back-EMF and average on-load torque. Meanwhile, the

stator gap changes the equivalent combination of slot and pole number, which increases the harmonic contents of air-gap flux density and peak cogging torque significantly. Due to the uneven equivalent air-gap distribution, stator gap leads to unbalanced three phase back-EMFs (both amplitudes and phase angles) and self- and mutual-inductances. In addition, the stator gap increases the total motor loss due to the increase of rotor PM loss. The results also show that the influence on total loss is small when the stator gap less than 1mm. The tooth tip mainly affects the self-inductance of the motor with 1mm stator gap.

The influence of another manufacturing tolerance, i.e. misalignment of two split parts, on the electromagnetic performance of 6s/2p HSPM motor with toroidal winding and diametrically magnetized PM rotor has also been analyzed. It shows that the misalign of two stator parts mainly affects the uneven equivalent air-gap and symmetry of winding configuration, which leads to unbalanced three phase back-EMFs, especially phase angles, and self- and mutual-inductances. In addition, the misalignment increases the total motor loss due to the increase of rotor PM loss and has negligible influence on stator iron loss.

REFERENCES

[1] T. Noguchi, Y. Takata, Y. Yamashita, Y. Komatsu, and S. Ibaraki, "220,000 r/min, 2kW PM motor drive for turbocharger," *IEEJ Trans. Ind. Appl.*, vol. 125, no. 9, pp. 854–861, Aug. 2005.

[2] J. D. Ede, Z. Q. Zhu, and D. Howe, "Rotor resonances of high-speed permanent-magnet brushless machines," *IEEE Trans. Ind. Appl.*, vol. 38, no. 6, pp. 1542–1548, Nov. 2002.

[3] C. Zwyssig, J. W. Kolar, W. Thaler, and M. Vohrer, "Design of a 100 W, 500000 RPM permanent-magnet generator for mesoscale gas turbines," in *Proc. 14th IAS Annu. Meeting. Conf. Rec. Ind. Appl. Conf.*, Hong Kong, 2005, pp. 253–260.

[4] A. Gilson, F. Dubas, D. Depernet, and C. Espanet, "Comparison of high-speed PM machine topologies for electrically-assisted turbocharger applications," in *Proc. Int. Conf. Electr. Mach. Syst. (ICEMS)*, Chiba, Japan, 2016, pp. 1–5.

[5] M. Schuck, A. Da Silva Fernandes, D. Steinert, and J. W. Kolar, "A high speed millimeter-scale slotless bearlngless slice motor," in *Proc. IEEE Int. Electr. Mach. Drives Conf. (IEMDC)*, May 2017, pp. 1–7.

[6] F. Cheng, H. Xu, and S. Xue, "Study on the design method of high speed permanent magnet synchronous machine," in *Proc. Int. Conf. Electr. Mach. Syst.*, Beijing, China, Aug. 2011, pp. 1–6.

[7] F. Wang, D. Zhang, J. Xing, and Y. Xu, "Study on air friction loss of high speed PM machine," in *Proc. IEEE Int. Conf. Ind. Technol.*, Gippsland, VIC, Australia, Feb. 2009, pp. 1–4.

[8] J. Dong, Y. Huang, L. Jin, B. Guo, H. Lin, J. Dong, M. Cheng, and H. Yang, "Electromagnetic and thermal analysis of open-circuit air cooled high-speed permanent magnet machines with gramme ring windings," *IEEE Trans. Magn.*, vol. 50, no. 11, pp. 1–4, Nov. 2014.

[9] X. Zhang, W. Li, H. Zhang, C. Gerada, M. Galea, and J. Li, "Topology investigation on high speed PM generator with back wound windings," in *Proc. IEEE 25th Int. Symp. Ind. Electron. (ISIE)*, Santa Clara, CA, USA, Jun. 2016, pp. 234–239.

[10] Z. Q. Zhu, D. Ishak, and D. Howe, "Modular permanent magnet brushless machines having a fractional number of slots per pole-influence of stator teeth and back-iron," in *Proc. Int. Conf. Electr. Mach. Syst. (ICEMS)*, Nagasaki, Japan, 2006, pp. 1–4.

[11] Z. Q. Zhu and Y. X. Li, "Modularity techniques in high performance permanent magnet machines and applications," *CES Trans. Electr. Mach. Syst.*, vol. 2, no. 1, pp. 93–103, Mar. 2018.

[12] F. Libert and J. Soulard, "Manufacturing methods of stator cores with concentrated windings," in *Proc. 3rd IET Int. Conf. Power Electron., Mach. Drives (PEMD)*, Apr. 2006, pp. 676–680.

[13] Z. Chen, "A modular, permanent-magnet generator for variable speed wind turbines," in *Proc. 7th Int. Conf. Electr. Mach. Drives*, 1995, pp. 453–457.

[14] E. Spooner, A. C. Williamson, and G. Catto, "Modular design of permanent-magnet generators for wind turbines," *IEE Proc.-Electr. Power Appl.*, vol. 143, no. 5, pp. 388–395, Sep. 1996.

[15] E. Spooner and A. Williamson, "Modular, permanent-magnet wind turbine generators," in *Proc. Conf. Rec. IEEE Ind. Appl. Conf. 31st IAS Annu. Meeting*, Oct. 1996, pp. 497–502.

[16] E. Spooner and C. Williamson, "Electromagnetic machine with at least one pair concentric rings having modularized magnets and yokes," U.S. Patent 5 844 341, Dec. 1, 1998.

[17] G. J. Li, Z. Q. Zhu, M. Foster, and D. Stone, "Comparative studies of modular and unequal tooth PM machines either with or without tooth tips," *IEEE Trans. Magn.*, vol. 50, no. 7, pp. 1–10, Jul. 2014.

[18] G. J. Li and Z. Q. Zhu, "Analytical modeling of modular and unequal tooth width surface-mounted permanent magnet machines," *IEEE Trans. Magn.*, vol. 51, no. 9, pp. 1–9, Sep. 2015.

[19] Z. Q. Zhu, Z. Azar, and G. Ombach, "Influence of additional air gaps between stator segments on cogging torque of permanent-magnet machines having modular stators," *IEEE Trans. Magn.*, vol. 48, no. 6, pp. 2049–2055, Jun. 2012.

[20] F. Xu, T. R. He, Z. Q. Zhu, Y. Wang, S. Cai, H. Bin, D. Wu, L. M. Gong, and J. T. Chen, "Influence of slot number on electromagnetic performance of 2-pole high-speed permanent magnet motors with toroidal windings," in *Proc. 15th Int. Conf. Ecological Vehicles Renew. Energies (EVER)*, Monaco, Sep. 2020, pp. 1–7.

[21] Y. Pang, Z. Q. Zhu, and D. Howe, "Analytical determination of optimal split ratio for permanent magnet brushless motors," *IEE Proc.-Electr. Power Appl.*, vol. 153, no. 1, pp. 7–13, Jan. 2006.

[22] G. Bertotti, "General properties of power losses in soft ferromagnetic materials," *IEEE Trans. Magn.*, vol. TMAG-24, no. 1, pp. 621–630, Jan. 1988.

[23] K. Atallah, Z. Q. Zhu, and D. Howe, "An improved method for predicting iron losses in brushless permanent magnet DC drives," *IEEE Trans. Magn.*, vol. 28, no. 5, pp. 2997–2999, Sep. 1992.

[24] J. Ma and Z. Q. Zhu, "Magnet eddy current loss reduction in a 3-slot 2-pole permanent magnet machine," in *Proc. IEEE Int. Electr. Mach. Drives Conf. (IEMDC)*, Miami, FL, USA, May 2017, pp. 1–8.
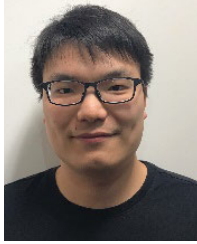
F. XU received the B.Eng. degree in electrical engineering from Nanjing Forestry University, Jiangsu, China, in 2015, and the M.Sc. degree in electrical engineering from The University of Sheffield, Sheffield, U.K. in 2016, where she is currently pursuing the Ph.D. degree in electrical engineering with the Department of Electronic and Electrical Engineering. Her major research interests include the design and analysis of permanent magnet brushless motors for high-speed application.

Z. Q. ZHU (Fellow, IEEE) received the B.Eng. and M.Sc. degrees in electrical and electronic engineering from Zhejiang University, Hangzhou, China, in 1982 and 1984, respectively, and the Ph.D. degree in electrical and electronic engineering from The University of Sheffield, Sheffield, U.K., in 1991. Since 1988, he has been with The University of Sheffield, where he is currently a Professor with the Department of Electronic and Electrical Engineering, the Head of the Electrical Machines and Drives Research Group, the Royal Academy of Engineering/Siemens Research Chair, the Academic Director of Sheffield Siemens Gamesa Renewable Energy Research Centre, the Director of Midea Electrical Machines and Control Systems Research Centre, and the Director of Sheffield CRRC Electric Drives Technology Research Centre. His current major research interests include the design and control of permanent-magnet brushless machines and drives for applications ranging from electrified transportation through domestic appliance to renewable energy. He is a Fellow of the Royal Academy of Engineering and the IET, U.K. He was a recipient of the 2019 IEEE Industry Applications Society Outstanding Achievement Award and the 2021 IEEE Nikola Tesla Award.

T. R. HE received the B.Eng. degree in electrical engineering from the Harbin Institute of Technology, Harbin, China, in 2014, and the M.Sc. degree in electrical engineering from The University of Sheffield, Sheffield, U.K. in 2017, where he is currently pursuing the Ph.D. degree in electrical engineering with the Department of Electronic and Electrical Engineering. From 2014 to 2016, he was an Engineer with Shanghai Electric Wind Power Group Company Ltd., Shanghai, China. His major research interests include the design and analysis of high-speed permanent magnet brushless motor.

Y. WANG received the B.Eng. and M.Sc. degrees in electrical engineering from the Nanjing University of Aeronautics and Astronautics, Nanjing, China, in 2013 and 2016, respectively, and the Ph.D. degree in electrical engineering from The University of Sheffield, Sheffield, U.K., in 2019.

Since 2019, he has been with the Sheffield Siemens Gamesa Renewable Energy Research Centre, The University of Sheffield, where he is currently a Research Associate. His research interests include the analysis and design of novel permanent magnet machines for high-speed and wind power generation applications. Since August 2019, he has been appointed as the Chair of the IEEE University of Sheffield Student Branch Joint IAS/PELS Chapter.

H. BIN received the B.Eng. and M.Sc. degrees in electrical engineering from Tongji University, Shanghai, China, in 2002 and 2015, respectively. He is currently working with the Midea Group Corporate Research Center, Shanghai. His current research interests include high-speed BLDC motor drives and PWM converters.

D. WU (Member, IEEE) received the M.Sc. degree in electrical engineering from the Huazhong University of Science and Technology, Wuhan, China, in 2011, and the Ph.D. degree in electronic and electrical engineering from The University of Sheffield, Sheffield, U.K., in 2015. Since 2011, he has been working with Midea Welling Motor Technology (Shanghai) Company Ltd., Shanghai, China. He is currently the Head of the Motor Development Department, Welling, Midea Group. His major research interests include the design and analysis of permanent-magnet brushless machines.

L. M. GONG (Senior Member, IEEE) received the B.Eng. and M.Sc. degrees in electrical engineering from the Huazhong University of Science and Technology, Wuhan, China, in 2001 and 2004, respectively, and the Ph.D. degree in electrical and electronic engineering from The University of Sheffield, Sheffield, U.K., in 2012. From 2004 to 2008, he was a Research Engineer with Emerson Network Power Company Ltd., Shenzhen, China, working to develop general purpose ac drives. Since 2012, he has been with Midea Welling Motor Technology (Shanghai) Company Ltd. His research interests include control of permanent-magnet brushless machines and power electronics.

J. T. CHEN (Senior Member, IEEE) received the B.Eng. and M.Sc. degrees in electrical engineering from the Huazhong University of Science and Technology, Wuhan, China, in 2001 and 2004, respectively, and the Ph.D. degree in electrical engineering from The University of Sheffield, Sheffield, U.K., in 2009. From 2004 to 2006, he was an Engineer with Delta Electronics (Shanghai) Company, Ltd., Shanghai, China. He is currently a General Manager of Midea Automotive Components Ltd., and also with the Midea Shanghai Motors and Drives Research Center, Shanghai. His major research interest includes the design of permanent magnet machines.

• • •